Dymore User's Manual
Unsteady Aerodynamics

Contents

1 Kinematics interface

An airstation location involves two distinct elements: its geometric position characterized by its position vector, $\underline{x}_a$, and its curvilinear coordinate, s_i, along the composite curve that defines the lifting line. An orthonormal basis $\mathcal{A} = (\bar{a}_1, \bar{a}_2, \bar{a}_3)$ defines the orientation of the airfoil. At each airstation, an airfoil is defined; it lies in a plane passing

through the airstation and normal to unit vector $\bar{a}_1$. Vector $\bar{a}_2$ points towards the leading edge of the airfoil and $\bar{a}_3$ towards the direction of positive lift. The configuration of the problem is depicted in fig. 1

The motion of the airfoil will be determined by the motion of the beam to which it is rigidly connected. Curvilinear coordinate s_i determines point **S** along the composite curve that defines the geometry of the lifting line. Hence, this point belongs to a beam element; fig. 1 shows the airfoil attached to a four noded beam element, for example. The position and velocity of point **S** will be determined from the corresponding nodal values of the finite element discretization. Since point **S** is a point on the reference line of a beam, the plane of the cross-section at that point is also defined. An orthonormal basis $\mathcal{E} = (\bar{e}_1, \bar{e}_2, \bar{e}_3)$ defines the orientation of the beam's cross-sectional plane. The plane of the cross-section passes through point **S** and is normal to unit vector $\bar{e}_1$, the tangent to the composite curve. Vectors $\bar{e}_2$ and $\bar{e}_2$ defined the plane of the cross-section. The orientations of bases $\mathcal{A}$ and $\mathcal{E}$ do not necessarily coincide. The orientation and angular velocity of the cross-sectional plane at point **S** will be determined from the corresponding nodal values of the finite element discretization.

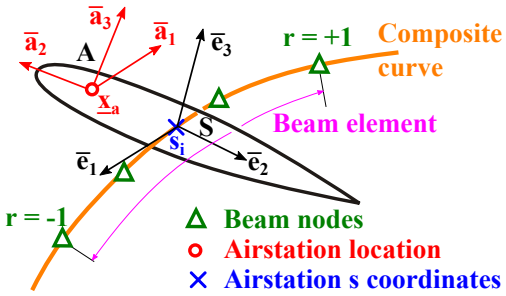

Figure 1: Configuration of an airfoil at an airstation and associated beam element.

The kinematic interface computes the following kinematic quantities: the inertial position vector of point **A**, the inertial orientation tensor of basis $\mathcal{A}$, the inertial velocity and acceleration vectors of point **A**, and the inertial angular velocity and acceleration vectors of basis $\mathcal{A}$. This computation proceeds in two step: first, the kinematic quantities associated with point **S**, the point on the reference line of the beam, are determined, and second, the kinematic quantities of the airstation at point **A** are computed.

1.1 Structural kinematic quantities

The first step towards the determination of the kinematic quantities of the airfoil is the evaluation of the kinematic quantities at point **S**, the point located on the reference line of the beam at curvilinear coordinate s_i. Let $\underline{u}^k$, $k = 1, 2, \ldots K$ be the displacements of the nodes of the beam element, see fig. 1, and K the number of nodes of the element. The shape functions of the element are defined in terms of a local variable, $r \in [-1, +1]$, within the element [1]. Let $r = r_i$ determine the position of point **S**. The displacement, $\underline{u}_s$, of point **S** is now interpolated using standard finite element techniques to find

$$\underline{u}_s(t) = \underline{u}(r = r_i, t) = \sum_{k=1}^{K} h^k(r_i)\, \underline{u}^k(t), \tag{1}$$

where $h^k(r)$ are the shape functions of the beam element. The time history of the displacement of point **S** can be determined since the above equation can be used at any time t.

Let $\underline{r}^k$, $k = 1, 2, \ldots K$ be the rotation parameter vector of the nodes of the beam element; using a similar interpolation process, the rotation parameter vector, $\underline{r}_s(t)$, at point **S** is determined easily. The rotation tensor, $\underline{\underline{R}}_s(t)$, that determines the rotation of the beam's cross-section is computed from these rotation parameter vectors. Within the framework of the finite element discretization of the structure, both nodal displacements, velocities, and accelerations are evaluated. From the nodal velocities, the linear velocities, $\underline{v}_s(t)$, and angular velocities, $\underline{\omega}_s(t)$, of point **S** are obtained from a similar interpolation procedure. Finally, the linear accelerations, $\underline{\dot{v}}_s$, and angular accelerations, $\underline{\dot{\omega}}_s(t)$, of point **S** are obtained.

In summary, the structural kinematic quantities determined in this first step are: *(1)* the inertial displacement, velocity, and acceleration vectors of point **S**, denoted $\underline{u}_s(t)$, $\underline{v}_s(t)$, and $\underline{\dot{v}}_s(t)$, respectively, *(2)* the inertial rotation tensor, $\underline{\underline{R}}_s(t)$, of the beam's cross-section at point **S**, and *(3)* the inertial angular velocity and accelerations vectors of the same cross-section, denoted $\underline{\omega}_s(t)$ and $\underline{\dot{\omega}}_s(t)$, respectively. All these vectors and tensors are resolved in inertial basis $\mathcal{I} = (\bar{\imath}_1, \bar{\imath}_2, \bar{\imath}_3)$.

1.2 Airstation kinematic quantities

Once the structural kinematic quantities of point **S** and associated beam cross-section have been determined, the kinematic quantities of the airfoil are derived.

Figure 2 shows the system in the reference and present configurations. In the reference configuration, the inertial position vector of point **S** is given as $\underline{u}_{s0}$, and the inertial orientation of the cross-section is given by rotation tensor $\underline{\underline{R}}_{s0}$. Similarly, the inertial position vector of the airstation is given as $\underline{u}_{a0}$, and the inertial orientation of the airfoil basis is given by the rotation tensor $\underline{\underline{R}}_{a0}$.

The position vector of the airstation with respect to point **S** is now

$$\underline{d}_0 = \underline{u}_{a0} - \underline{u}_{s0}. \tag{2}$$

To compute the kinematic quantities of the airstation, it is assumed that the airstation, the airfoil basis, and their structural counterparts undergo a **rigid body motion** characterized by translation $\underline{u}_s$ and rotation $\underline{\underline{R}}_s$. In view of fig. 2, the inertial position of the airstation is found easily

$$\underline{u}_a = \underline{u}_{s0} + \underline{u}_s + \underline{d} = \underline{u}_{s0} + \underline{u}_s + \underline{\underline{R}}_s \ \underline{d}_0, \tag{3}$$

where the last equality follows from the rigid body motion assumption: $\underline{d} = \underline{\underline{R}}_s \ \underline{d}_0$. Similarly, because the airfoil basis, $\mathcal{A}$, undergoes rotation $\underline{\underline{R}}_s$,

$$\underline{\underline{R}}_a = \underline{\underline{R}}_s \underline{\underline{R}}_{a0}. \tag{4}$$

With the help of the rigid body motion assumption, the velocity and acceleration vectors of the airstation are found as

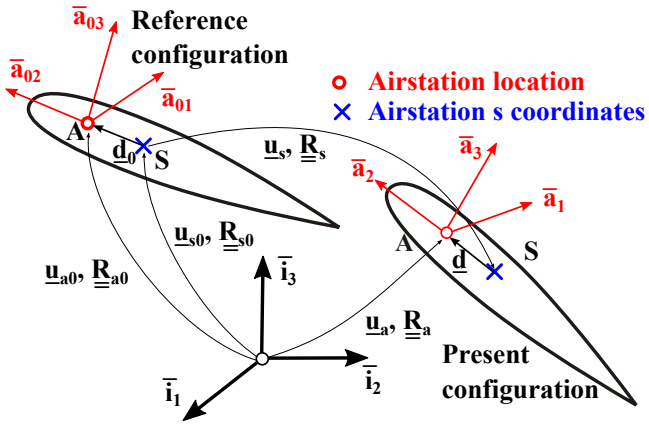

Figure 2: Configuration of an airfoil in the reference and present configurations.

$$\underline{v}_a = \underline{v}_s + \tilde{\omega}_s \underline{d}, \tag{5a}$$

$$\underline{\dot{v}}_a = \underline{\dot{v}}_s + (\dot{\tilde{\omega}}_s + \tilde{\omega}_s \tilde{\omega}_s)\underline{d}, \tag{5b}$$

and the angular velocity and acceleration vectors of bases $\mathcal{E}$ and $\mathcal{A}$ are, of course, identical

$$\underline{\omega} = \underline{\omega}_a = \underline{\omega}_s \tag{6a}$$

$$\underline{\dot{\omega}} = \underline{\dot{\omega}}_a = \underline{\dot{\omega}}_s \tag{6b}$$

2 Relative flow velocity

The formulation of two-dimensional, unsteady aerodynamic theories typically requires the velocity of the flow with respect to the airfoil, which simply writes

$$\underline{\hat{v}}_a = \underline{V}_\infty + \underline{\lambda} - \underline{v}_a, \tag{7}$$

where $\underline{V}_\infty$ is the far field flow velocity, assumed to be of constant magnitude and orientation and $\underline{\lambda}$ the average inflow velocity over the airfoil. When using the internal aerodynamic model, airstations must be located at the airfoil's quarter-chord point, to comply with the usual aerodynamic convention; hence, eq. (7) gives the relative velocity of the flow with respect to the airfoil quarter-chord point.

As shown in fig. 3, the components of the relative velocity vector resolved in basis $\mathcal{A}$ are denoted

$$\underline{\hat{v}}_a^* = \underline{\underline{R}}_a^T \underline{\hat{v}}_a = \begin{Bmatrix} U_1 \\ -U_2 \\ U_3 \end{Bmatrix}, \tag{8}$$

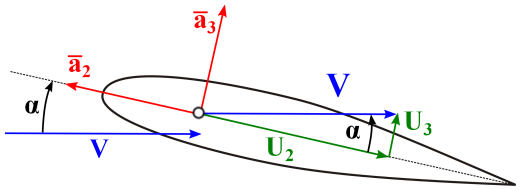

Figure 3: Relative velocity of the flow with respect to the quarter-chord point.

where notation $(\cdot)^*$ indicates components of vectors and tensors resolved in basis $\mathcal{A}$. Note the minus sign for the U_2 component: to comply with the sign convention used in aerodynamic theories, the velocity component parallel to the chord direction is taken positive towards the trailing edge. Velocity components U_1, U_2, and U_3 are sometimes denoted U_R, U_T, and U_P, respectively, indicating the radial, tangent and perpendicular components of the relative flow.

Next, the relative acceleration of the flow is evaluated as $\underline{\dot{\hat{v}}}_a^* = \underline{\underline{R}}_a^T \tilde{\omega}^T \underline{\hat{v}}_a + \underline{\underline{R}}_a^T \underline{\dot{\hat{v}}}_a = \tilde{\omega}^{*T} \underline{\hat{v}}_a^* - \underline{\underline{R}}_a^T \underline{\dot{v}}_a$. Equation (7) was used to obtain the last equality and the following approximation was made: $\underline{\dot{\hat{v}}}_a \approx -\underline{\dot{v}}_a$ because the far field flow, including the inflow, is assumed to be of constant magnitude and orientation. The components of the relative acceleration vector resolved in basis $\mathcal{A}$ are denoted

$$\underline{\hat{a}}_a^* = \begin{Bmatrix} A_1 \\ -A_2 \\ A_3 \end{Bmatrix}. \tag{9}$$

It follows that $A_3 = \omega_2^* U_1 + \omega_1^* U_2 - \dot{v}_{a3}^*$, and hence

$$A_3 \approx \omega_1^* U_2 - \dot{v}_{a3}^*, \tag{10}$$

where the effect of the radial flow velocity was ignored.

When dealing with two-dimensional unsteady aerodynamic theories, the analysis often focuses on flow components U_2 and U_3 in the plane of airfoil, and component U_1 along the wing or blade is ignored, as shown in fig. 3. The flow velocity, V, is defined as the resultant of components U_2 and U_3,

$$V = \sqrt{U_2^2 + U_3^2}. \tag{11}$$

The angle of attack, α, is then defined by the following relationships

$$U_2 = V \cos\alpha; \quad U_3 = V \sin\alpha. \tag{12}$$

The relative velocities at the airfoil quarter-, mid- and three-quarter-chord points, denoted $\underline{\hat{v}}_a^{\rm qc}$, $\underline{\hat{v}}_a^{\rm mc}$ and $\underline{\hat{v}}_a^{\rm tc}$, respectively, are sometimes used in unsteady aerodynamics theories, as illustrated in fig. 4. For instance, the unsteady aerodynamic developed by Peters, see section 3, is based on the relative velocity of the flow with respect to the airfoil mid-chord point. Since the airfoil is assumed to be rigid, the following relationships must hold: $\underline{\hat{v}}_a^{\rm qc} = \underline{\hat{v}}_a^{\rm mc} + \tilde{\omega}_a \underline{\eta}$ and $\underline{\hat{v}}_a^{\rm tc} = \underline{\hat{v}}_a^{\rm mc} - \tilde{\omega}_a \underline{\eta}$, where $\underline{\eta}$ is the relative position vector of the quarter-chord point with respect to the mid-chord point.

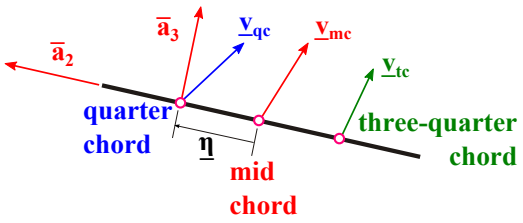

Figure 4: Velocity vectors at the airfoil quarter-, mid- and three-quarter-chord points.

3 Two dimensional unsteady aerodynamics of Peters *et al.*

3.1 Summary of the theory

This section summarizes the state-space unsteady aerodynamic theory developed by Peters and coworkers for flexible airfoils. Full details of the derivation of the the theory can be found in Peters and Johnson [2], Peters *et al.* [3], and Ahaus and Peters [4].

Figure 5 depicts the general coordinate system used for the development of the theory. The airfoil is undergoing an arbitrary unsteady motion through a mass of still air. At a given instant, the velocity of the air as viewed by an airfoil attached observer is denoted u_0 along the positive x direction and v_0 along the positive y direction. The velocity gradient, denoted v_1, is counted positive for a nose-up rotation of the airfoil. The origin of the coordinate system is located at the airfoil's mid-chord location, and hence, spans $-b \le x \le +b$. The deformation of the airfoil, denoted $h(x,t)$ is assumed to remain small, *i.e.*, $h/b \ll 1$, $\partial h/\partial x \ll 1$, and $\partial h/\partial t \ll u_0$.

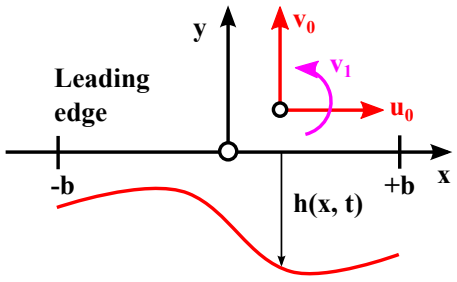

Figure 5: General airfoil coordinate system.

All the variables of the problem are expanded in terms of the Glauert angle, ϕ, defined as

$$x = b\cos\phi, \quad -b \le x \le +b, \quad 0 \le \phi \le \pi. \tag{13}$$

For direct flow, the trailing and leading edges correspond to $\phi = 0$ and π, respectively.

The bound circulation per unit length on the airfoil is expanded in terms of the Glauert angle as

$$\gamma_b = 2\left[\frac{\gamma_s}{\sin\phi} - \frac{\gamma_0\cos\phi}{\sin\phi} + \sum_{n=1}^{\infty}\gamma_n \sin n\phi\right], \tag{14}$$

and a similar expansion holds for the pressure drop across the airfoil

$$\Delta P = 2\rho\left[\frac{\tau_s}{\sin\phi} - \frac{\tau_0\cos\phi}{\sin\phi} + \sum_{n=1}^{\infty}\tau_n \sin n\phi\right], \tag{15}$$

where ρ is the air density. The first two terms in these expansions are the singular potential functions that allow suction peaks at either end of the airfoil, when appropriate.

The total bound circulation, denoted Γ

$$\Gamma = 2\pi b(\gamma_s + \gamma_1/2). \tag{16}$$

Following a similar pattern, the other variable of the problem are

$$\lambda = \sum_{n=0}^{\infty} \lambda_n \cos n\phi, \tag{17a}$$

$$h = \sum_{n=0}^{\infty} h_n \cos n\phi, \tag{17b}$$

$$\partial h/\partial x = \sum_{n=0}^{\infty} h_n \frac{n \sin n\phi}{b \sin \phi} = \sum_{n=1,3,5}^{\infty} \frac{n h_n}{b} + \sum_{n=1}^{\infty} \left[\sum_{k=n+1,n+3,}^{\infty} \frac{2k h_k}{b} \right] \cos n\phi, \tag{17c}$$

Of course, inverse relationships can be found by using the orthogonality properties of trigonometric function. For instance,

$$h_0 = \frac{1}{\pi} \int_0^{\phi} h \ \mathrm{d}\theta, \tag{18a}$$

$$h_i = \frac{2}{\pi} \int_0^{\phi} h \cos i\theta \ \mathrm{d}\theta, \quad i = 1, 2, \ldots, \infty. \tag{18b}$$

The basic equations of potential flow theory then imply

$$u_0 \gamma_s = \tau_s, \tag{19a}$$

$$u_0 \gamma_0 = \tau_0, \tag{19b}$$

$$b(\dot{\gamma}_0 - \frac{\dot{\gamma}_2}{2}) + u_0 \gamma_1 = \tau_1 - \frac{\dot{\Gamma}}{\pi}, \tag{19c}$$

$$\frac{b}{2n}(\dot{\gamma}_{n-1} - \dot{\gamma}_{n+1}) + u_0 \gamma_n = \tau_n - \frac{\dot{\Gamma}}{n\pi}, \quad n \geq 2. \tag{19d}$$

The inflow states are related to the time derivative of the total bound circulation,

$$b(\dot{\lambda}_0 - \frac{\dot{\lambda}_2}{2}) + u_0 \lambda_1 = \frac{\dot{\Gamma}}{\pi}, \tag{20a}$$

$$\frac{b}{2n}(\dot{\lambda}_{n-1} - \dot{\lambda}_{n+1}) + u_0 \lambda_n = \frac{\dot{\Gamma}}{n\pi}, \quad n \geq 2. \tag{20b}$$

The airfoil loads are then expressed as

$$\tau_0 = u_0(w_0 - \lambda_0), \tag{21a}$$

$$\tau_1 = u_0 w_1 + b\left(\dot{w}_0 - \frac{\dot{w}_2}{2}\right), \tag{21b}$$

$$\tau_n = u_0 w_n + \frac{b}{2n}\left(\dot{w}_{n-1} - \dot{w}_{n+1}\right), \quad n > 2. \tag{21c}$$

The generalized loads acting on the airfoil are defined as

$$L_n = -\int_{-b}^{+b} \Delta P \cos n\phi \ \mathrm{d}x = -\int_0^{\pi} \Delta P \cos n\phi \ b \sin \phi \mathrm{d}\phi. \tag{22}$$

Introducing the expansion for the pressure drop across the airfoil, eq. (15), then yields

$$\frac{L_0}{2\pi\rho b} = -(f\tau_0 + \frac{\tau_1}{2}), \tag{23a}$$

$$\frac{L_1}{2\pi\rho b} = \frac{1}{2}(\tau_0 - \frac{\tau_2}{2}), \tag{23b}$$

$$\frac{L_n}{2\pi\rho b} = \frac{1}{4}(\tau_{n-1} - \tau_{n+1}), \quad n \geq 2. \tag{23c}$$

3.1.1 Kutta condition and reverse flow parameter

The Kutta condition can be expressed as

$$\tau_s = f\tau_0, \tag{24}$$

where f is the reverse flow parameter, which is designed to enforce the vanishing pressure drop at the trailing edge of the airfoil. Because the trailing edge can change position depending on the sign of u_0, different values of this parameter can be selected

$$f = \begin{cases} 1 & \text{ignore reversed flow regime,} \\ u_0/|u_0| & \text{fully reversed flow regime,} \\ u_0/\sqrt{u_0^2 + (v_0 + \dot{h}_0 - \lambda_0)^2} & \text{soft reversed flow regime} \end{cases} \tag{25}$$

If $f = 1$, the vanishing of the pressure drop across the airfoil is enforced at $x = b$; this is equivalent to *ignoring the reversed flow regime*. If f changes sign with u_0, the vanishing of the pressure drop across the airfoil switches to $x = -b$ when u_0 changes sign; this corresponds to a fully reversed flow regime. The last option enforces a smooth transition between the direct and reversed flow regimes with symmetrical suction peaks at $x = \pm b$ when $u_0 = 0$; the reverse flow parameter can be interpreted as $f = \cos\alpha$, where α is the angle of attack at mid-chord.

3.1.2 Loading components

Introducing the total velocity components into eqs. (21) yields the components of the pressure drop across the airfoil and eqs. (23) finally give the generalized loads acting on the airfoil as

$$\frac{L_0}{2\pi\rho b} = -f u_0(w_0 - \lambda_0) - \frac{u_0}{2} w_1 - \frac{b}{2}(\dot{w}_0 - \frac{\dot{w}_2}{2}), \tag{26a}$$

$$\frac{L_1}{2\pi\rho b} = \frac{u_0}{2}(w_0 - \lambda_0) - \frac{u_0}{4} w_2 - \frac{b}{16}(\dot{w}_1 - \dot{w}_3), \tag{26b}$$

$$\frac{L_2}{2\pi\rho b} = \frac{u_0}{4}(w_1 - w_3) + \frac{b}{4}(\dot{w}_0 - \frac{\dot{w}_2}{2}) - \frac{b}{24}(\dot{w}_2 - \dot{w}_4), \tag{26c}$$

$$\frac{L_n}{2\pi\rho b} = \frac{u_0}{4}(w_{n-1} - w_{n+1}) + \frac{b}{8(n-1)}(\dot{w}_{n-2} - \dot{w}_n) - \frac{b}{8(n+1)}(\dot{w}_n - \dot{w}_{n+2}), \quad n \geq 3. \tag{26d}$$

The total bound circulation is

$$\frac{\Gamma}{2\pi b} = f(w_0 - \lambda_0) + \frac{1}{2} w_1 - \frac{1}{2}\lambda_1. \tag{27}$$

The components of the total velocity are expressed in term of the frame motion, u_0, v_0, and v_1 and the components of airfoil deformation, h_n, as

$$w_0 = v_0 + \dot{h}_0 + u_0 \sum_{k=1,3}^{\infty} \frac{k h_k}{b}, \tag{28a}$$

$$w_1 = v_1 + \dot{h}_1 + 2u_0 \sum_{k=2,4}^{\infty} \frac{k h_k}{b}, \tag{28b}$$

$$w_n = \quad \dot{h}_n + 2u_0 \sum_{k=n+1,n+3}^{\infty} \frac{k h_k}{b}, \quad n \geq 2. \tag{28c}$$

3.1.3 Summary of the key equations

Introducing the total velocity components given by eq. (28) into eqs. (26) gives the generalized loads acting on the airfoil in terms of the frame motions and airfoil deformation parameters

$$\frac{L_0}{2\pi\rho b^2} = -\frac{1}{2}(\dot{v}_0 + \ddot{h}_0 - \frac{\ddot{h}_2}{2}) - \frac{u_0}{b}\Upsilon - \frac{u_0}{b}(v_1 + \dot{h}_1) - \frac{1}{2}(\frac{\dot{u}_0}{b} h_1 - \frac{u_0}{b} v_1), \tag{29a}$$

$$\frac{L_1}{2\pi\rho b^2} = -\frac{1}{16}(\dot{v}_1 + \ddot{h}_1 - \ddot{h}_3) + \frac{1}{2}\frac{u_0}{b}(v_0 + \dot{h}_0 - \lambda_0) - \frac{1}{2}\frac{u_0}{b}\dot{h}_2 + \frac{1}{2}\frac{u_0^2}{b^2} h_1 - \frac{1}{4}\frac{\dot{u}_0}{b} h_2, \tag{29b}$$

$$\frac{L_2}{2\pi\rho b^2} = \frac{1}{4}(\dot{v}_0 + \ddot{h}_0) - \frac{\ddot{h}_2}{6} + \frac{\ddot{h}_4}{24} + \frac{1}{2}\frac{u_0}{b}(\frac{v_1}{2} + \dot{h}_1 - \dot{h}_3) + \frac{u_0^2}{b^2} h_2 + \frac{1}{4}\frac{\dot{u}_0}{b}(h_1 - h_3), \tag{29c}$$

$$\frac{L_n}{2\pi\rho b^2} = \frac{\ddot{h}_{n-2}}{8(n-1)} - \frac{n\ddot{h}_n}{4(n^2-1)} + \frac{\ddot{h}_{n+2}}{8(n+1)} + \frac{1}{2}\frac{u_0}{b}(\dot{h}_{n-1} - \dot{h}_{n+1}) + \frac{1}{2}\frac{u_0^2}{b^2} n h_n + \frac{1}{4}\frac{\dot{u}_0}{b}(h_{n-1} - h_{n+1}). \tag{29d}$$

The drag force, denoted D_0, is

$$\frac{D_0}{2\pi\rho b} = -(v_0 + \dot{h}_0 - \lambda_0)\Upsilon + \sum_{k=1}^{\infty}\left[\frac{\ddot{h}_{k-1} - \ddot{h}_{k+1}}{4} + \frac{u_0}{b} k\dot{h}_k + \frac{1}{2}\frac{\dot{u}_0}{b} k h_k\right] h_k + \left[\frac{\dot{v}_0}{2} + \frac{\ddot{h}_0}{4} + \frac{u_0}{b}\frac{v_1}{2}\right] h_1 + \frac{1}{4}\dot{v}_1 h_2, \tag{30}$$

and finally, the total bound circulation is

$$\frac{\Gamma}{2\pi b} = \Upsilon + \frac{1}{2}(v_1 + \dot{h}_1 - \lambda_1). \tag{31}$$

In these equations, the following notation was defined

$$\Upsilon = f(v_0 + \dot{h}_0 - \lambda_0) + \frac{u_0}{b}\left[f\sum_{k=1,3,5}^{\infty} kh_k + \sum_{k=2,4,6}^{\infty} kh_k\right]. \tag{32}$$

3.1.4 Summary of notation and sign conventions

Peters theory was developed in the general airfoil coordinate system depicted in fig. 5 and eqs. (22) imply the positive sign conventions for loading components L_0 and L_1 shown in the upper portion of fig. 6. Note that the loading components are evaluated at the airfoil's mid-chord location.

In airfoil theory, it is customary to compute the lift, denoted L, aerodynamic moment, denoted M, and lift induced drag, denoted D, with respect to the airfoil's quarter-chord. Typically, the lift is counted positive up, the aerodynamic moment is positive when causing a nose-up rotation, and the drag positive towards the leading edge, as depicted in the lower portion of fig. 6. The following relationships follow

$$L = -L_0, \tag{33a}$$

$$M = b(L_1 + \frac{L_0}{2}) = bL_1 - \frac{b}{2}L, \tag{33b}$$

$$D = -D_0, \tag{33c}$$

and will be used to transform the loading components obtained from Peters theory to the lift, moment, and drag components commonly used in airfoil theory.

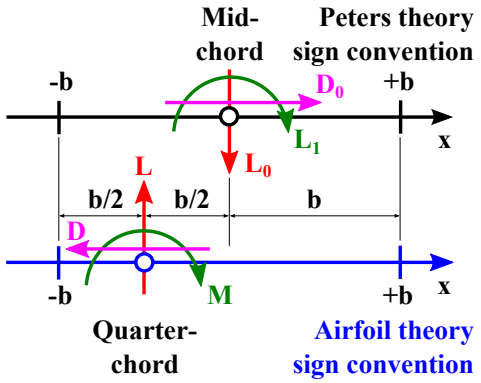

Figure 6: Sign conventions for Peters and airfoil theories.

In section 2, the relative velocity of the air with respect to the airfoil was evaluated, and the component of this relative velocity vector resolved in basis $\mathcal{A}$ were denoted U_2 and U_3 along unit vectors $\bar{\imath}_2$ and $\bar{\imath}_3$, respectively, as shown in fig. 3. The following notational transformations follow,

$$u_0 = U_2, \tag{34a}$$

$$v_0 - \lambda_0 = U_3, \tag{34b}$$

$$v_1 = b\omega_1. \tag{34c}$$

$$\dot{v}_0 = A_3 = \omega_1 U_2 - \dot{v}_{a3}, \tag{34d}$$

where the last equality results from eq. (10). In the following sections, all vector and tensor components are resolved in basis $\mathcal{A}$; consequently, superscript $(\cdot)^*$ is dropped to simplify the writing.

With these new definitions, the loading components on the airfoil given by eqs. (29) become

$$\frac{L_0}{2\pi\rho b^2} = -\left[\frac{U_2}{b}\left(fU_3 + \frac{U_2}{b}\Sigma\right)\right] + \left[-U_2\omega_1 - \frac{U_2}{b}\left(f\dot{h}_0 + \dot{h}_1\right) - \frac{\dot{U}_2}{b}\frac{h_1}{2}\right] + \left[\frac{1}{2}\dot{v}_{a3} - \frac{\ddot{h}_0}{2} + \frac{\ddot{h}_2}{4}\right], \tag{35a}$$

$$\frac{L_1}{2\pi\rho b^2} = \left[\frac{1}{2}\frac{U_2}{b}U_3 + \frac{U_2^2}{b^2}\frac{h_1}{2}\right] + \left[\frac{U_2}{b}\frac{\dot{h}_0 - \dot{h}_2}{2} - \frac{\dot{U}_2}{b}\frac{h_2}{4}\right] + \left[-\frac{b}{16}\dot{\omega}_1 - \frac{\ddot{h}_1}{16} + \frac{\ddot{h}_3}{16}\right], \tag{35b}$$

$$\frac{L_2}{2\pi\rho b^2} = \left[\frac{U_2^2}{b^2}\frac{2h_2}{2}\right] + \left[\frac{1}{2}U_2\omega_1 + \frac{U_2}{b}\frac{\dot{h}_1 - \dot{h}_3}{2} + \frac{\dot{U}_2}{b}\frac{h_1 - h_3}{4}\right] + \left[-\frac{1}{4}\dot{v}_{a3} + \frac{\ddot{h}_0}{4} - \frac{\ddot{h}_2}{6} + \frac{\ddot{h}_4}{24}\right], \tag{35c}$$

$$\frac{L_n}{2\pi\rho b^2} = \left[\frac{U_2^2}{b^2}\frac{nh_n}{2}\right] + \left[\frac{U_2}{b}\frac{\dot{h}_{n-1} - \dot{h}_{n+1}}{2} + \frac{\dot{U}_2}{b}\frac{h_{n-1} - h_{n+1}}{4}\right] + \left[\frac{\ddot{h}_{n-2}}{8(n-1)} - \frac{n\ddot{h}_n}{4(n^2-1)} + \frac{\ddot{h}_{n+2}}{8(n+1)}\right]. \tag{35d}$$

The drag force, given by eq. (30), becomes

$$\begin{aligned}\frac{D_0}{2\pi\rho b} = &-\left[U_3\left(fU_3 + \frac{U_2}{b}\Sigma\right)\right] + \left[\omega_1 U_2 h_1 - \left(2fU_3 + \frac{U_2}{b}\Sigma + f\dot{h}_0\right)\dot{h}_0 + \sum_{k=1}^{\infty}\left(\frac{U_2}{b}k\dot{h}_k + \frac{\dot{U}_2}{b}\frac{kh_k}{2}\right)h_k\right] \\ &+ \left[\left(\frac{\ddot{h}_0}{4} - \frac{1}{2}\dot{v}_{a3}\right)h_1 + \frac{b}{4}\dot{\omega}_1 h_2 + \sum_{k=1}^{\infty}\frac{\ddot{h}_{k-1} - \ddot{h}_{k+1}}{4}h_k\right],\end{aligned} \tag{36}$$

and finally, the total bound circulation is

$$\frac{\Gamma}{2\pi b} = \left[f U_3 + \frac{U_2}{b}\Sigma \right] + \left[\frac{b}{2}\omega_1 + f\dot{h}_0 + \frac{\dot{h}_1}{2} - \frac{\lambda_1}{2} \right]. \tag{37}$$

In the evaluation of the total bound circulation, the inflow gradient, λ_1, is often neglected because it is not easily evaluated. In these equations, scalar Σ was defined as

$$\Sigma = f \sum_{k=1,3,5}^{\infty} k h_k + \sum_{k=2,4,6}^{\infty} k h_k. \tag{38}$$

4 The rigid airfoil

For a rigid airfoil, all deformation parameters vanish, *i.e.*, $h_i = \dot{h}_i = \ddot{h}_i = 0$, which implies $\Sigma = 0$. Peters theory, summarized by eqs. (35), (36), and (37) yield the airfoil loading components as

$$L = a_0 f\ \rho b\ U_2 U_3 + a_0 \rho b^2 U_2 \omega_1 - a_0 \rho \frac{b^2}{2}\dot{v}_{a3}, \tag{39a}$$

$$M = a_0 \rho \frac{b^2}{2} U_2 U_3 - a_0 \rho \frac{b^4}{16}\dot{\omega}_1 - \frac{b}{2}L. \tag{39b}$$

In the expression for the lift, the first term represents the steady lift component, the second the aerodynamic damping in pitch, and the last the inertial effect. The drag force is

$$D = a_0 f\ \rho b U_3^2, \tag{40}$$

and the total bound circulation

$$\Gamma = a_0 f\ b U_3 + a_0 \frac{b^2}{2}\omega_1 - a_0 \frac{b}{2}\lambda_1. \tag{41}$$

The theoretical value of the slope of the lift curve, 2π, was replaced by a_0 in the above expressions.

4.1 Corrections for wind tunnel measurements

The **steady** components of the lift and drag forces are obtained from eqs. (39a) and (39b), respectively, as

$$L^{\mathrm{s}} = a_0 f\ \rho b\ U_2 U_3, \tag{42a}$$

$$D^{\mathrm{s}} = a_0 f\ \rho b\ U_3^2, \tag{42b}$$

$$M^{\mathrm{s}} = a_0 \rho \frac{b^2}{2} U_2 U_3 - \frac{b}{2} L^{\mathrm{s}}. \tag{42c}$$

These expressions were derived for a thin airfoil in a two-dimensional inviscid, incompressible flow, and hence, are approximate in nature.

Steady wind tunnel measurements have been acquired for numerous airfoils and the corresponding lift, drag, and moment coefficients are available in tabulated form as functions of angle of attack and Mach numbers. It is also possible to use computational fluid dynamics codes to compute the same coefficients based on theories that remove many of the assumptions made in Peters theory. It then seems appropriate to correct eqs. (42) to make sure they yield the wind tunnel measurements for steady flows.

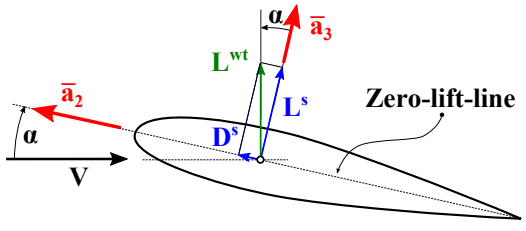

Figure 7: Test set-up for an airfoil in a wind tunnel.

Figure 7 depicts the typical experimental setup used in wind tunnel experiments. The airfoil is set at an angle of attack α with respect to the steady, far-field flow velocity, V. The angle of attack is defined as the angle between the far-field flow velocity direction and the zero-lift-line of the airfoil. The force in the direction normal to the flow is defined as

$$L^{\mathrm{wt}} = c_\ell(\alpha, \mathcal{M})\ \rho b V^2, \tag{43}$$

where c_ℓ are the experimentally measured *lift coefficients*. Typically, these coefficients are tabulated as functions of the angle of attack, α, and Mach number, $\mathcal{M}$.

The lift and drag forces acting on the airfoil in a steady flow are given by eqs. (42a) and (42b), respectively and can be manipulated in the following manner

$$L^{\rm s} = \rho b\ a_0 f\ U_3 U_2 = \rho b V^2\ a_0 f\ \frac{U_3}{V}\frac{U_2}{V} = \rho b V^2 (a_0 f \sin\alpha)\cos\alpha, \tag{44a}$$

$$D^{\rm s} = \rho b\ a_0 f\ U_3 U_3 = \rho b V^2\ a_0 f\ \frac{U_3}{V}\frac{U_3}{V} = \rho b V^2 (a_0 f \sin\alpha)\sin\alpha, \tag{44b}$$

respectively, where α is the quarter-chord angle of attack defined by eq. (12) and V the far field flow velocity in the plane of the airfoil given by eq. (11). A cursory look at fig. 7 reveals that the steady lift and drag forces defined by eqs. (42a) and (42b), respectively, are the projections of the lift measured in the wind tunnel along axes $\bar{a}_3$ and $\bar{a}_2$, respectively, *i.e.*, $L^{\rm s} = L^{\rm wt}\cos\alpha$ and $D^{\rm s} = L^{\rm wt}\sin\alpha$. Clearly, wind tunnel test measurements and theoretical predictions become identical if the following choice is made

$$c_\ell(\alpha, \mathcal{M})\ = a_0 f \sin\alpha. \tag{45}$$

Next, correction of the steady quarter-chord moment is also derived. The expression for the steady moment is given by eq. (42c) and can be manipulated in the following manner

$$M^{\rm s}_{\rm qc} = a_0 \rho \frac{b^2}{2}(1-f) U_2 U_3. \tag{46}$$

For direct flow, $f = 1$, and the quarter-chord moment vanishes, as expected. In the wind tunnel test, a non-vanishing quarter-chord steady moment is measured and the corresponding moment coefficient, denoted c_m, is defined as

$$M^{\rm wt}_{\rm qc} = c_m(\alpha, \mathcal{M})\ 2\rho b^2 V^2. \tag{47}$$

Here again, the moment coefficient, c_m, is now a function of the angle of attack, α, and Mach number, $\mathcal{M}$.

In summary, after corrections to account for wind tunnel measurements, the steady lift, drag, and moment expressions become

$$\hat{L}^{\rm s} = c_\ell(\alpha, \mathcal{M})\ \rho b V U_2, \tag{48a}$$

$$\hat{D}^{\rm s} = c_\ell(\alpha, \mathcal{M})\ \rho b V U_3, \tag{48b}$$

$$\hat{M}^{\rm s}_{\rm qc} = c_m(\alpha, \mathcal{M})\ 2\rho b^2 V^2. \tag{48c}$$

4.2 Unsteady aerodynamic loads

The **unsteady** components of lift, drag, and moment are obtained from eqs. (39a) and (39b), respectively, as

$$L^{\rm us} = a_0 \rho b^2 U_2 \omega_1 - a_0 \rho \frac{b^2}{2}\dot{v}_{a3}, \tag{49a}$$

$$D^{\rm us} = 0, \tag{49b}$$

$$M^{\rm us}_{\rm qc} = -a_0 \rho \frac{b^4}{16}\dot{\omega}_1 - \frac{b}{2}L^{\rm us}, \tag{49c}$$

where ω_1 the pitch rate of the airfoil, counted positive about axis $\bar{a}_1$, *i.e.*, it is positive for a nose-up rotation.

4.3 Corrections to for wind tunnel drag measurements

Because Peters theory is based on a two-dimensional inviscid, incompressible flow around a thin airfoil, it does not predict the viscous drag. Here again, wind tunnel test measurements can be used to supplement the theory.

Figure 8 shows the drag force, $D^{\rm wt}$, measured in the wind tunnel and expressed as

$$D^{\rm wt} = c_d(\alpha, \mathcal{M})\ \rho b V^2, \tag{50}$$

where c_d is the *drag coefficient*. The components of the drag force along axes $-\bar{a}_2$ and $\bar{a}_3$ are denoted S_2 and S_3, respectively, and can be expressed as

$$S_2 = c_d\ \rho b V^2 \cos\alpha = c_d\ \rho b V U_2, \tag{51a}$$

$$S_3 = c_d\ \rho b V^2 \sin\alpha = c_d\ \rho b V U_3. \tag{51b}$$

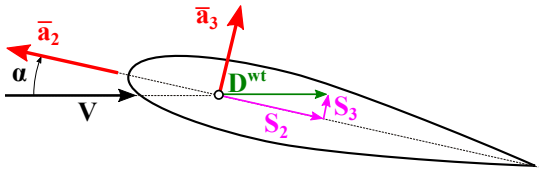

Figure 8: Measurement of the drag force in the wind tunnel.

In the presence of flow along the blade, the flow velocity component along axis $\bar{a}_1$ is denoted U_1. Defining the resultant flow velocity $V_R^2 = U_1^2 + U_2^2$, the associated skin friction drag is $D^{\rm sf} = c_{d0}\ \rho b V_R^2$, where c_{d0} is the skin friction drag coefficient, estimated to be equal to the drag coefficient at zero lift force. The components of this force along axes $\bar{a}_1$ and $-\bar{a}_2$ are $S_1 = c_{d0}\ \rho b V_R U_1$ and $S_2 = c_{d0}\ \rho b V_R U_2$, respectively.

The drag forces acting on the airfoil are obtained by summing up the pressure and skin friction drag components. The net force along axis $-\bar{a}_2$ will be $S_2 = c_d\ \rho b V U_2 + c_{d0}\ \rho b V_R U_2$. Clearly, this expression is incorrect because it double counts the skin friction drag, and hence, it will be corrected as $S_2 = c_d\ \rho b V U_2 - c_{d0}\ \rho b U_2^2 + c_{d0}\ \rho b V_R U_2$. This last expression recovers wind tunnel measurements in the absence of radial flow. In summary, the pressure and skin friction drag components are

$$S_1 = c_{d0}(\alpha, \mathcal{M})\ \rho b V_R U_1, \tag{52a}$$
$$S_2 = c_d(\alpha, \mathcal{M})\ \rho b V U_2 + c_{d0}(\alpha, \mathcal{M})\ \rho b (V_R - U_2) U_2, \tag{52b}$$
$$S_3 = c_d(\alpha, \mathcal{M})\ \rho b V U_3. \tag{52c}$$

4.4 Summary

Peters unsteady aerodynamic theory, corrected by wind tunnel test measurements, predicts aerodynamic forces along axes $\bar{a}_1$, $\bar{a}_2$, and $\bar{a}_3$, denoted F_1, F_2, and F_3, respectively and moments about axes $\bar{a}_1$, $\bar{a}_2$, and $\bar{a}_3$, denoted M_1, M_2, and M_3, respectively. The expressions for these forces and moments are found by summing up their corrected steady counterparts, eq. (48), unsteady components, eq. (49), and the drag and skin friction components, eq. (52), to find

$$F_1 = \qquad\qquad\qquad S_1, \tag{53a}$$
$$F_2 = f_{\rm tl}\hat{D}^{\rm s} \qquad\qquad - S_2, \tag{53b}$$
$$F_3 = f_{\rm tl}\hat{L}^{\rm s} \quad + f_{\rm tl}L^{\rm us} \quad + S_3, \tag{53c}$$
$$M_1 = f_{\rm tl}\hat{M}^{\rm s}_{\rm qc} + f_{\rm tl}M^{\rm us}_{\rm qc}, \tag{53d}$$
$$M_2 = 0, \tag{53e}$$
$$M_3 = 0. \tag{53f}$$

The tip loss correction factor, denoted $f_{\rm tl}$, was introduced in these expressions.

4.5 Relationship of Peters' formulation to Theodorsen's theory

The unsteady aerodynamic formulation described in the previous section is closely related to Theodorsen's theory, as described by Bisplinghoff *et al.* [5].

$$\hat{L} = \pi\rho b^2\left[\ddot{h} + V\dot{\hat{\alpha}} - ba\ddot{\hat{\alpha}}\right] + 2\pi\rho V b C(k)\left[\dot{h} + V\hat{\alpha} + b(\frac{1}{2} - a)\dot{\hat{\alpha}}\right], \tag{54a}$$
$$\hat{M}_{\rm mc} = \pi\rho b^2\left[ba\ddot{h} - Vb(\frac{1}{2} - a)\dot{\hat{\alpha}} - b^2(\frac{1}{8} + a^2)\ddot{\hat{\alpha}}\right] + 2\pi\rho V b^2(a + \frac{1}{2})C(k)\left[\dot{h} + V\hat{\alpha} + b(\frac{1}{2} - a)\dot{\hat{\alpha}}\right], \tag{54b}$$

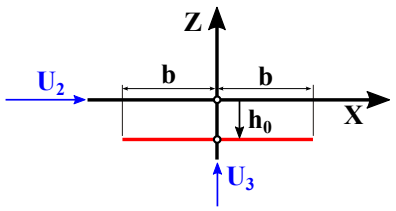

Figure 9: Peters' formulation. U_2 is the uniform x velocity, and U_3 is the uniform z velocity. $h_0(t)$ is the motion in the z direction.

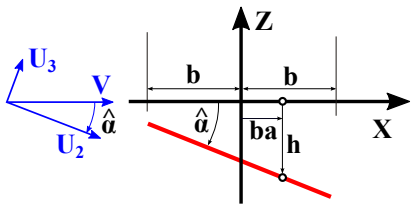

Figure 10: Theodorsen's theory. V is the flow velocity. $h(t)$ is the downward displacement of the axis ($x = ba$) of rotation, $\hat{\alpha}(t)$.

In Peters' formulation, the effect of the trailed vortices is taken into account through the inflow velocity $\underline{\lambda}$ that is added to the far filed flow velocity, whereas in Theodorsen's theory, the same vorticity enters the formulation through the lift deficiency function $C(k)$. Hence, identical expressions should be recovered from the two approaches by setting $\underline{\lambda} = 0$ and $C(k) = 1$ in Peters' and Theodorsen's formulations, respectively. Since Peters' formulation is based on the relative velocity of the flow with respect to the airfoil mid-chord point, we set $a = 0$ in Theodorsen's theory. For a

flat plate the slope of the lift curve $a_0 = 2\pi$. The quasi-steady lift, $\hat{L}$, and pitching moment, $\hat{M}_{\rm mc}$, expressions in Theodorsen's theory are

$$\hat{L} = \frac{a_0}{2}\rho b^2\left[\ddot{h} + V\dot{\hat{\alpha}}\right] + a_0\rho V b\left[\dot{h} + V\hat{\alpha} + \frac{b}{2}\dot{\hat{\alpha}}\right], \tag{55a}$$

$$\hat{M}_{\rm mc} = \frac{a_0}{2}\rho b^2\left[-V\frac{b}{2}\dot{\hat{\alpha}} - \frac{b^2}{8}\ddot{\hat{\alpha}}\right] + a_0\rho V\frac{b^2}{2}\left[\dot{h} + V\hat{\alpha} + \frac{b}{2}\dot{\hat{\alpha}}\right], \tag{55b}$$

respectively, where $h(t)$ is the mid-chord heaving measured positive downwards, $\hat{\alpha}(t)$ the airfoil geometric pitch angle, and V the flow velocity. Both theories are valid for small angles of attack, *i.e.*, $V \approx U_2$, $V\hat{\alpha} \approx U_3$, $V\dot{\hat{\alpha}} = (V\hat{\alpha})^{\cdot} \approx \dot{U}_3$ and $h \approx h_0$. Also, $\omega_1 = \dot{\hat{\alpha}}$ is the airfoil pitch rate. With these approximations, the lift and mid-chord pitching moment then become

$$\hat{L} = a_0\rho U_2 b\left(\dot{h}_0 + U_3\right) + \frac{a_0}{2}\rho b^2\left(\ddot{h}_0 + \dot{U}_3\right) + a_0\rho U_2\frac{b^2}{2}\omega_1, \tag{56a}$$

$$\hat{M}_{\rm mc} = \frac{a_0}{2}\rho b^2\left[-U_2\frac{b}{2}\omega_1 - \frac{b^2}{8}\dot{\omega}_1\right] + a_0\rho U_2\frac{b^2}{2}\left[(\dot{h}_0 + U_3) + \frac{b}{2}\omega_1\right] = -\frac{a_0}{16}\rho b^4\dot{\omega}_1 + \frac{a_0}{2}\rho b^2 U_2\left(\dot{h}_0 + U_3\right), \tag{56b}$$

Note that we can incorporate $\dot{h}_0$ into U_3, and $\ddot{h}_0$ into $\dot{U}_3$, since $\dot{h}_0$ and U_3 are both the velocities of the flow with respect to the airfoil in Peters' formulation. The first term in the lift expression is the steady lift, identical to eq. (42a), whereas the last two terms represent the unsteady lift, identical to eq. (49a). This shows the equivalence of the lift expressions in the two theories. To show the equivalence of the pitching moment expressions, the mid-chord moment given by Theodorsen is computed at the quarter-chord as $M_{\rm qc} = \hat{M}_{\rm mc} - b\hat{L}/2$ to yield

$$M_{\rm qc} = \hat{M}_{\rm mc} - \frac{b}{2}\hat{L} = -\frac{a_0}{16}\rho b^4\dot{\omega}_1 + \frac{a_0}{2}\rho b^2 U_2\left(\dot{h}_0 + U_3\right) - \frac{b}{2}\hat{L}. \tag{57}$$

Introducing the expression for the lift, eq. (56a), then leads to

$$M_{\rm qc} = -a_0\rho\frac{b^4}{16}\dot{\omega}_1 - \frac{b}{2}\left[a_0\rho\frac{b^2}{2}(\ddot{h}_0 + \dot{U}_3) + a_0\rho U_2\frac{b^2}{2}\omega_1\right]. \tag{58}$$

Since the bracketed term of this equation is identical to the unsteady lift given by eq. (49a), Theodorsen's quarter-chord moment becomes equivalent to its counterpart in Peters' formulation, eq. (49c).

5 Airfoil with a trailing edge flap

The results presented in the previous section summarize the application of Peters theory to a rigid airfoil. Peters theory, however, also applies to deformable airfoils, as presented in section 3. Airfoils with trailing edge flaps can be viewed as deformable airfoils, as shown in fig. 11. The main wing moves with the rigid body coordinate system and the trailing flap has a mid-span defection denoted ϵ and an angular deflection denoted δ; positive sign conventions are depicted in the figure.

5.1 Kinematics of the trailing edge flap

The deflection of the deformable airfoil is written as

$$h(\phi) = \begin{cases} \epsilon + [b\cos\phi - b(1+d)/2]\delta & 0 \le \phi \le \theta, \\ 0 & \theta \le \phi \le \pi, \end{cases} \tag{59}$$

where θ is the Glauert angle defining the position of the trailing edge flap and db the distance this hinge is located aft the airfoil's mid-chord. The configuration depicted in fig. 11 shows a discontinuity between the main wing and the flap. For typical constructions, the flap is connected to the wing by means of brackets and revolute joints. At these attachment points, the main wing and flap connect without discontinuity; on the other hand, small discontinuities are likely to occur at intermediate points. When the main wing and flap connect smoothly, the flap mid-point deflection is not independent of its angular deflection

$$\epsilon = \frac{b}{2}(1-d)\delta. \tag{60}$$

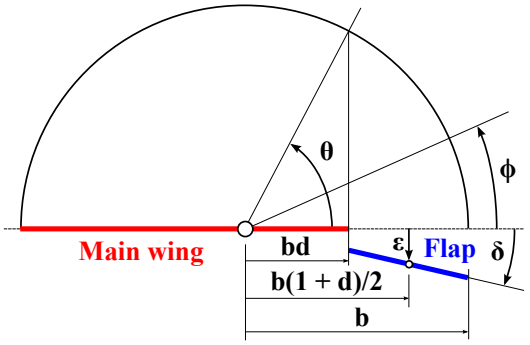

Figure 11: Configuration of the trailing edge flap.

The components of the Glauert expansion of the camber line of the airfoil are found by introducing the airfoil displacement field (59) into the generic expression (18) to find

$$h_0 = \frac{\theta}{\pi}\epsilon + \frac{b}{\pi}\left[\sin\theta - \frac{1+d}{2}\theta\right]\delta, \tag{61a}$$

$$h_1 = \frac{2\sin\theta}{\pi}\epsilon + \frac{b}{\pi}\left[\theta - (1+d)\sin\theta + \frac{\sin 2\theta}{2}\right]\delta, \tag{61b}$$

$$h_n = \frac{2\sin n\theta}{n\pi}\epsilon + \frac{b}{\pi}\left[\frac{\sin(n-1)\theta}{n-1} - (1+d)\frac{\sin n\theta}{n} + \frac{\sin(n+1)\theta}{n+1}\right]\delta, \quad n \geq 2. \tag{61c}$$

It is convenient to introduce the following matrix

$$\underline{T} = \frac{b}{\pi}\begin{Bmatrix} \sin\theta - \theta\cos\theta \\ \theta - \sin\theta\cos\theta \\ \dfrac{\sin 3\theta}{3} - \dfrac{2}{2}\cos\theta\sin 2\theta + \dfrac{\sin\theta}{1} \\ \vdots \\ \dfrac{\sin(n+1)\theta}{n+1} - \dfrac{2}{n}\cos\theta\sin n\theta + \dfrac{\sin(n-1)\theta}{n-1} \end{Bmatrix}, \tag{62}$$

and using eq. (60), the airfoil displacement components given by eq. (61) now become

$$\underline{h} = \underline{T}\delta. \tag{63}$$

The flap hinge moment, denoted H, is evaluated as

$$H = \underline{T}^T\underline{L}, \tag{64}$$

where $\underline{L}$ is the array of airfoil loading components, whose entries are defined by eqs. (35).

5.2 The airfoil loading components

The loading components defined in eqs. (35) for a general deformable airfoil apply to the present airfoil with a trailing edge flap. Because the flap kinematics is characterized by the single flap angular deflection, constant Σ is given by eq. (38) and the loading components become

$$\frac{L_0}{2\pi\rho b^2} = -\left[\frac{U_2}{b}\left(fU_3 + \frac{U_2}{b}\Sigma\right)\right] + \left[-U_2\omega_1 - \frac{U_2}{b}\left(f\dot{h}_0 + \dot{h}_1\right) - \frac{\dot{U}_2}{b}\frac{h_1}{2}\right] + \left[\frac{1}{2}\dot{v}_{a3} - \frac{\ddot{h}_0}{2} + \frac{\ddot{h}_2}{4}\right], \tag{65a}$$

$$\frac{L_1}{2\pi\rho b^2} = \left[\frac{1}{2}\frac{U_2}{b}U_3 + \frac{U_2^2}{b^2}\frac{h_1}{2}\right] + \left[\frac{U_2}{b}\frac{\dot{h}_0 - \dot{h}_2}{2} - \frac{\dot{U}_2}{b}\frac{h_2}{4}\right] + \left[-\frac{b}{16}\dot{\omega}_1 - \frac{\ddot{h}_1}{16} + \frac{\ddot{h}_3}{16}\right], \tag{65b}$$

$$\frac{L_2}{2\pi\rho b^2} = \left[\frac{U_2^2}{b^2}\frac{2h_2}{2}\right] + \left[\frac{1}{2}U_2\omega_1 + \frac{U_2}{b}\frac{\dot{h}_1 - \dot{h}_3}{2} + \frac{\dot{U}_2}{b}\frac{h_1 - h_3}{4}\right] + \left[-\frac{1}{4}\dot{v}_{a3} + \frac{\ddot{h}_0}{4} - \frac{\ddot{h}_2}{6} + \frac{\ddot{h}_4}{24}\right], \tag{65c}$$

$$\frac{L_n}{2\pi\rho b^2} = \left[\frac{U_2^2}{b^2}\frac{nh_n}{2}\right] + \left[\frac{U_2}{b}\frac{\dot{h}_{n-1} - \dot{h}_{n+1}}{2} + \frac{\dot{U}_2}{b}\frac{h_{n-1} - h_{n+1}}{4}\right] + \left[\frac{\ddot{h}_{n-2}}{8(n-1)} - \frac{n\ddot{h}_n}{4(n^2-1)} + \frac{\ddot{h}_{n+2}}{8(n+1)}\right]. \tag{65d}$$

The drag force given by eq. (36) becomes

$$\begin{aligned}\frac{D_0}{2\pi\rho b} = &-\left[U_3\left(fU_3 + \frac{U_2}{b}\Sigma\right)\right] + \left[\omega_1 U_2 h_1 - \left(2fU_3 + \frac{U_2}{b}\Sigma + f\dot{h}_0\right)\dot{h}_0 + \sum_{k=1}^{\infty}\left(\frac{U_2}{b}k\dot{h}_k + \frac{\dot{U}_2}{b}\frac{kh_k}{2}\right)h_k\right] \\ &+ \left[\left(\frac{\ddot{h}_0}{4} - \frac{1}{2}\dot{v}_{a3}\right)h_1 + \frac{b}{4}\dot{\omega}_1 h_2 + \sum_{k=1}^{\infty}\frac{\ddot{h}_{k-1} - \ddot{h}_{k+1}}{4}h_k\right],\end{aligned} \tag{66}$$

and finally, the total bound circulation, given by eq. (37) is

$$\frac{\Gamma}{2\pi b} = \left[fU_3 + \frac{U_2}{b}\Sigma\right] + \left[\frac{b}{2}\omega_1 + f\dot{h}_0 + \frac{\dot{h}_1}{2} - \frac{\lambda_1}{2}\right]. \tag{67}$$

5.3 Corrections for wind tunnel measurements

The **steady** components of airfoil loading are obtained from eqs. (65) as

$$\frac{L_0^{\rm s}}{2\pi\rho b^2} = -\frac{U_2}{b}(fU_3 + \frac{U_2}{b}\Sigma), \tag{68a}$$

$$\frac{L_1^{\rm s}}{2\pi\rho b^2} = \frac{1}{2}\frac{U_2}{b}U_3 + \frac{U_2^2}{b^2}\frac{h_1}{2}, \tag{68b}$$

$$\frac{L_2^{\rm s}}{2\pi\rho b^2} = \frac{U_2^2}{b^2}\frac{2h_2}{2}, \tag{68c}$$

$$\frac{L_n^{\rm s}}{2\pi\rho b^2} = \frac{U_2^2}{b^2}\frac{nh_n}{2}, \tag{68d}$$

and the drag force becomes

$$\frac{D_0^{\rm s}}{2\pi\rho b} = -U_3(fU_3 + \frac{U_2}{b}\Sigma), \tag{69}$$

Using a procedure similar to that outlined in eqs. (44a) and (44b), the steady components of lift and drag become

$$L^{\rm s} = \rho b\left(a_0 fU_3 + a_0\frac{\Sigma}{b}U_2\right)U_2 = \rho bV^2\left(a_0 f\frac{U_3}{V} + a_0\frac{\Sigma}{b}\frac{U_2}{V}\right)\frac{U_2}{V} = \rho bV^2\left(a_0 f\sin\alpha + a_0\frac{\Sigma}{b}\cos\alpha\right)\cos\alpha, \tag{70a}$$

$$D^{\rm s} = \rho b\left(a_0 fU_3 + a_0\frac{\Sigma}{b}U_2\right)U_3 = \rho bV^2\left(a_0 f\frac{U_3}{V} + a_0\frac{\Sigma}{b}\frac{U_2}{V}\right)\frac{U_3}{V} = \rho bV^2\left(a_0 f\sin\alpha + a_0\frac{\Sigma}{b}\cos\alpha\right)\sin\alpha, \tag{70b}$$

respectively, where α is the angle of attack defined by eq. (12) and V the far field flow velocity in the plane of the airfoil given by eq. (11). A cursory look at fig. 7 reveals that the steady lift and drag forces defined by eqs. (42a) and (42b), respectively, are the projections of the lift measured in the wind tunnel along axes $\bar{a}_3$ and $\bar{a}_2$, respectively, *i.e.*, $L^{\rm s} = L^{\rm wt}\cos\alpha$ and $D^{\rm s} = L^{\rm wt}\sin\alpha$. Clearly, wind tunnel test measurements and theoretical predictions become identical if the following choice is made

$$c_\ell(\alpha, \mathcal{M}, \delta) = a_0 f\sin\alpha + a_0\frac{\Sigma}{b}\cos\alpha. \tag{71}$$

Note that the lift coefficient, c_ℓ, is now a function of the angle of attack, α, flap angular deflection, δ, and Mach number, $\mathcal{M}$.

Next, correction of the steady quarter-chord moment is also derived. The expression for the steady moment is given by eq. (42c) and can be manipulated in the following manner

$$M_{\rm qc}^{\rm s} = a_0\rho\frac{b^2}{2}(1-f)U_2U_3 + a_0\rho b(h_1 - \Sigma/2)U_2^2. \tag{72}$$

For direct flow, $f = 1$, and the quarter-chord moment is a function of the flap deflection only, as expected. In the wind tunnel test, a non-vanishing quarter-chord steady moment is measured and the corresponding moment coefficient, denoted c_m, is defined as

$$M_{\rm qc}^{\rm wt} = c_m\ 2\rho b^2V^2. \tag{73}$$

Here again, the moment coefficient, c_m, is now a function of the angle of attack, α, flap angular deflection, δ, and Mach number, $\mathcal{M}$. Finally, the static hinge moment is obtained from eq. (64) as $H^{\rm s} = \underline{T}^T\underline{L}^{\rm s}$. In the wind tunnel test, the flap hinge steady moment is measured and the corresponding moment coefficient, denoted c_h, is defined as

$$H^{\rm wt} = c_h(\alpha, \mathcal{M}, \delta)\ 2\rho b^2V^2. \tag{74}$$

In summary, after corrections to account for wind tunnel measurements, the steady lift, drag, moment, and hinge moment expressions become

$$\hat{L}^{\rm s} = c_\ell(\alpha, \mathcal{M}, \delta)\ \rho bVU_2, \tag{75a}$$

$$\hat{D}^{\rm s} = c_\ell(\alpha, \mathcal{M}, \delta)\ \rho bVU_3, \tag{75b}$$

$$\hat{M}_{\rm qc}^{\rm s} = c_m(\alpha, \mathcal{M}, \delta)\ 2\rho b^2V^2. \tag{75c}$$

$$\hat{H}^{\rm s} = c_h(\alpha, \mathcal{M}, \delta)\ 2\rho b^2V^2. \tag{75d}$$

5.4 Unsteady aerodynamic loads

The **unsteady** airfoil loading components are obtained from eqs. (65) as

$$\frac{L_0^{\text{us}}}{2\pi\rho b^2} = \left[-U_2\omega_1 - \frac{U_2}{b}\left(f\dot{h}_0 + \dot{h}_1\right) - \frac{\dot{U}_2}{b}\frac{h_1}{2}\right] + \left[\frac{1}{2}\dot{v}_{a3} - \frac{\ddot{h}_0}{2} + \frac{\ddot{h}_2}{4}\right], \tag{76a}$$

$$\frac{L_1^{\text{us}}}{2\pi\rho b^2} = \left[\frac{U_2}{b}\frac{\dot{h}_0 - \dot{h}_2}{2} - \frac{\dot{U}_2}{b}\frac{h_2}{4}\right] + \left[-\frac{b}{16}\dot{\omega}_1 - \frac{\ddot{h}_1}{16} + \frac{\ddot{h}_3}{16}\right], \tag{76b}$$

$$\frac{L_2^{\text{us}}}{2\pi\rho b^2} = \left[\frac{1}{2}U_2\omega_1 + \frac{U_2}{b}\frac{\dot{h}_1 - \dot{h}_3}{2} + \frac{\dot{U}_2}{b}\frac{h_1 - h_3}{4}\right] + \left[-\frac{1}{4}\dot{v}_{a3} + \frac{\ddot{h}_0}{4} - \frac{\ddot{h}_2}{6} + \frac{\ddot{h}_4}{24}\right], \tag{76c}$$

$$\frac{L_n^{\text{us}}}{2\pi\rho b^2} = \left[\frac{U_2}{b}\frac{\dot{h}_{n-1} - \dot{h}_{n+1}}{2} + \frac{\dot{U}_2}{b}\frac{h_{n-1} - h_{n+1}}{4}\right] + \left[\frac{\ddot{h}_{n-2}}{8(n-1)} - \frac{n\ddot{h}_n}{4(n^2-1)} + \frac{\ddot{h}_{n+2}}{8(n+1)}\right]. \tag{76d}$$

The unsteady flap hinge moment is then

$$H^{\text{us}} = \underline{T}^T \underline{L}^{\text{us}}. \tag{77}$$

The unsteady drag force is obtained from eq. (66) as

$$\begin{aligned}\frac{D_0^{\text{us}}}{2\pi\rho b} = &\left[\omega_1 U_2 h_1 - \left(2fU_3 + \frac{U_2}{b}\Sigma + f\dot{h}_0\right)\dot{h}_0 + \sum_{k=1}^{\infty}\left(\frac{U_2}{b}k\dot{h}_k + \frac{\dot{U}_2}{b}\frac{kh_k}{2}\right)h_k\right] \\ &+ \left[\left(\frac{\ddot{h}_0}{4} - \frac{1}{2}\dot{v}_{a3}\right)h_1 + \frac{b}{4}\dot{\omega}_1 h_2 + \sum_{k=1}^{\infty}\frac{\ddot{h}_{k-1} - \ddot{h}_{k+1}}{4}h_k\right],\end{aligned} \tag{78}$$

and finally, the total bound circulation follows from eq. (67) as

$$\frac{\Gamma^{\text{us}}}{2\pi b} = \left[\frac{b}{2}\omega_1 + f\dot{h}_0 + \frac{\dot{h}_1}{2} - \frac{\lambda_1}{2}\right]. \tag{79}$$

More specifically, the unsteady lift and aerodynamic moment at the quarter-chord are

$$L^{\text{us}} = a_0\rho b^2\left[U_2\omega_1 + \frac{U_2}{b}\left(f\dot{h}_0 + \dot{h}_1\right) + \frac{\dot{U}_2}{b}\frac{h_1}{2}\right] + a_0\rho b^2\left[-\frac{1}{2}\dot{v}_{a3} + \frac{\ddot{h}_0}{2} - \frac{\ddot{h}_2}{4}\right], \tag{80a}$$

$$M_{\text{qc}}^{\text{us}} = a_0\rho b^3\left[\frac{U_2}{b}\frac{\dot{h}_0 - \dot{h}_2}{2} - \frac{\dot{U}_2}{b}\frac{h_2}{4}\right] + a_0\rho b^3\left[-\frac{b}{16}\dot{\omega}_1 - \frac{\ddot{h}_1}{16} + \frac{\ddot{h}_3}{16}\right] - \frac{b}{2}L^{\text{us}}. \tag{80b}$$

The unsteady drag force is

$$\begin{aligned}D^{\text{us}} = &a_0\rho b\left[-\omega_1 U_2 h_1 + \left(2fU_3 + \frac{U_2}{b}\Sigma + f\dot{h}_0\right)\dot{h}_0 - \sum_{k=1}^{\infty}\left(\frac{U_2}{b}k\dot{h}_k + \frac{\dot{U}_2}{b}\frac{kh_k}{2}\right)h_k\right] \\ &- a_0\rho b\left[\left(\frac{\ddot{h}_0}{4} - \frac{1}{2}\dot{v}_{a3}\right)h_1 + \frac{b}{4}\dot{\omega}_1 h_2 + \sum_{k=1}^{\infty}\frac{\ddot{h}_{k-1} - \ddot{h}_{k+1}}{4}h_k\right],\end{aligned} \tag{81}$$

5.5 Corrections to for wind tunnel drag measurements

Because Peters theory is based on a two-dimensional inviscid, incompressible flow around a thin airfoil, it does not predict the viscous drag. Here again, wind tunnel test measurements can be used to supplement the theory. The pressure and skin friction drag components developed in section 4.3 can be added to the loading components for an airfoil with a trailing edge flap as well.

5.6 Summary

Peters unsteady aerodynamic theory, corrected by wind tunnel test measurements, predicts aerodynamic forces along axes $\bar{a}_1$, $\bar{a}_2$, and $\bar{a}_3$, denoted F_1, F_2, and F_3, respectively and moments about axes $\bar{a}_1$, $\bar{a}_2$, and $\bar{a}_3$, denoted M_1, M_2, and M_3, respectively. The expressions for these forces and moments are found by summing up their corrected steady

counterparts, eq. (75), unsteady components, eq. (80), and the drag and skin friction components, eq. (52), to find

$$F_1 = \qquad\qquad\qquad S_1, \tag{82a}$$
$$F_2 = f_{\mathrm{tl}}\hat{D}^{\mathrm{s}} + f_{\mathrm{tl}}D^{\mathrm{us}} - S_2, \tag{82b}$$
$$F_3 = f_{\mathrm{tl}}\hat{L}^{\mathrm{s}} + f_{\mathrm{tl}}L^{\mathrm{us}} + S_3, \tag{82c}$$
$$M_1 = f_{\mathrm{tl}}\hat{M}^{\mathrm{s}}_{\mathrm{qc}} + f_{\mathrm{tl}}M^{\mathrm{us}}_{\mathrm{qc}}, \tag{82d}$$
$$M_2 = 0, \tag{82e}$$
$$M_3 = 0. \tag{82f}$$

The tip loss correction factor, denoted f_{tl}, was introduced in these expressions. In addition, the flap hinge moment is the sum of its steady and unsteady components give by eqs. (75d) and (77), respectively,

$$H = f_{\mathrm{tl}}\hat{H}^{\mathrm{s}} + f_{\mathrm{tl}}H^{\mathrm{us}}. \tag{83}$$

6 The *ONERA EDLIN* dynamic stall model

Petot [6] extended the original *ONERA* model for application to the operating conditions encountered by helicopter airfoils. This model is based on delayed dynamic stall and second-order linear differential equations to compute the dynamic stall loads. The second-order differential equations that govern this model are in the following form

$$\frac{\mathrm{d}^2\Gamma}{\mathrm{d}t^2} + \eta\bar{V}\frac{\mathrm{d}\Gamma}{\mathrm{d}t} + \omega^2\bar{V}^2\Gamma = -V\omega^2\left(\bar{V}^2\Delta C + e\bar{V}\frac{\mathrm{d}\Delta C}{\mathrm{d}t}\right). \tag{84}$$

Three identical equations govern the lift, drag, and quarter-chord aerodynamic moment acting on the airfoil. In eq. (84), Γ is the circulation per unit span of the blade, ΔC is the difference in the aerodynamic coefficient between its linear static value extrapolated in the stalled region and its actual value at the angle of attack considered. The far field flow velocity is denoted V and $\bar{V} = V/b$, where b is the semi-chord length. Parameters η and e are nonlinear functions of ΔC_L defined as

$$\omega = \omega_0 + \omega_1\Delta C_L^2, \tag{85a}$$
$$\eta = \eta_0 + \eta_1\Delta C_L^2, \tag{85b}$$
$$e = e_0 + e_1\Delta C_L^2, \tag{85c}$$

parameters ω_0, ω_1, η_0, η_1, e_0, and e_1 characterize a given airfoil shape and are function of Mach number. Typical values of these parameters [6, 7] are listed in table 1. Note that coefficients ω, η, and e for the lift, drag, and quarter-chord moment acting on the airfoil are considered to be functions of ΔC_L only.

For the lift, drag, and quarter-chord aerodynamic moment problems, ΔC is defined by the following equations

$$\Delta C_L = c_\ell - (c_{\ell 0} + c_{\ell\alpha}\sin\alpha), \tag{86a}$$
$$\Delta C_D = c_d - \left(c_{d0} + c_{d\alpha}\sin^2\alpha\right), \tag{86b}$$
$$\Delta C_M = c_m - (c_{m0} + c_{m\alpha}\sin\alpha), \tag{86c}$$

respectively, as the difference in the aerodynamic coefficient between its linear static value extrapolated in the stalled region and its actual value at the angle of attack considered.

Let the solutions of eq. (84) for the lift, drag, and quarter-chord moment circulations be denoted Γ_L, Γ_D, and Γ_M, respectively. The corresponding airloads due to dynamic stall then follow as

$$L^{DS} = \rho V b\Gamma_L, \tag{87a}$$
$$D^{DS} = \rho V b\Gamma_D, \tag{87b}$$
$$M^{DS} = 2\rho V b^2\Gamma_M + bL^{DS}\frac{f-1}{2}, \tag{87c}$$

where the second term in the moment equation accounts for reverse flow effects through the reverse flow parameter defined by eq. (25).

6.1 Solution process

To solve eq. (84), the equation is recast in non-dimensional form as

$$\ddot{\bar{\Gamma}} + \eta\dot{\bar{\Gamma}} + \omega^2\bar{\Gamma} = -\omega^2\left(\Delta C + e\dot{\Delta C}\right), \tag{88}$$

Equation	Parameters	Range	Default Value
	ω_0	$[0.1, 0.4]$	0.2
	ω_1	$[0.0, 0.5]$	0.2
Lift	η_0	$[0.1, 0.4]$	0.3
	η_1	$[0.0, 0.6]$	0.2
	e_0	$[0.0]$	0.0
	e_1	$[-0.2, 0.0]$	-0.05
	τ_d	$[8.0]$	8.0
Drag	η_0	$[0.0, 0.5]$	0.25
	η_1	$[0.0, 0.6]$	0.0
	e_0	$[0.0]$	0.0
	e_1	$[0.0, -0.05]$	-0.015
	τ_d	$[0.0]$	0.0
Moment	η_0	$[0.0, 0.4]$	0.25
	η_1	$[0.0, 0.6]$	0.1
	e_0	$[0.0]$	0.0
	e_1	$[0.0, 0.06]$	0.01
	τ_d	$[2.0]$	2.0

Table 1: *ONERA* Dynamic Stall Coefficients

where $\bar{\Gamma} = \Gamma/V$ is the non-dimensional circulation, and notation $(\cdot)^{\cdot}$ indicates a derivative with respect to non-dimensional time $\tau = Vt/b$. Defining $\lambda = \bar{\Gamma}$ and $\mu = \dot{\lambda}$, and applying the central difference scheme to eq. (84) leads to

$$\frac{\mu_f - \mu_i}{\Delta\tau} + \eta_m \frac{\mu_f + \mu_i}{2} + \omega_m^2 \frac{\lambda_f + \lambda_i}{2} = -\omega_m^2 \left(\frac{\Delta C_f + \Delta C_i}{2} + e_m \frac{\Delta C_f - \Delta C_i}{\Delta\tau} \right), \tag{89}$$

where subscripts $(\cdot)_i$ and $(\cdot)_f$ denote value of variables at the beginning end end of the time step, respectively and subscript $(\cdot)_m = [(\cdot)_f + (\cdot)_i]/2$ a mid-point quantity. Using the same discretization for function μ yields $(\mu_i + \mu_f)/2 = (\lambda_f - \lambda_i)/\Delta\tau$, and hence, $\mu_f = 2(\lambda_f - \lambda_i)/\Delta\tau - \mu_i$. Introducing this result into eq. (89) and solving for λ_f yields

$$c_f \lambda_f = c_i \lambda_i + \frac{2}{\Delta\tau} 2\mu_i - d_f \Delta C_f - d_i \Delta C_i, \tag{90a}$$

$$\mu_f = \frac{2}{\Delta\tau}(\lambda_f - \lambda_i) - \mu_i, \tag{90b}$$

where $\Delta\tau = \bar{V}_m \Delta t$ and the following constants were defined

$$c_f = \frac{2}{\Delta\tau}\left(\frac{2}{\Delta\tau} + \eta_m\right) + \omega_m^2, \tag{91a}$$

$$c_i = \frac{2}{\Delta\tau}\left(\frac{2}{\Delta\tau} + \eta_m\right) - \omega_m^2, \tag{91b}$$

$$d_f = \omega_m^2 (1 + \frac{2}{\Delta\tau} e_m), \tag{91c}$$

$$d_i = \omega_m^2 (1 - \frac{2}{\Delta\tau} e_m). \tag{91d}$$

Coefficients d_f and d_i are corrected in the following manner

$$\bar{d}_{f,i} = \begin{cases} 0 & \tau \le \tau_d \\ d_{f,i} & \tau > \tau_d \end{cases} \tag{92}$$

where τ is the non-dimensional time, as computed by eq. (164), after the angle of attack exceeds the static stall value α_1, and τ_{d_i} is the non-dimensional time delay listed in table 1.

Once we solve for the circulations, we can compute the corresponding dynamic stall aerodynamic coefficients as

$$C_\ell^{DS} = \frac{\Gamma_\ell}{V}, \tag{93a}$$

$$C_d^{DS} = \frac{\Gamma_d}{V}, \tag{93b}$$

$$C_m^{DS} = \frac{\Gamma_m}{V} + \frac{1}{4} C_\ell^{DS} (f - 1). \tag{93c}$$

7 Leishman-Beddoes Unsteady aerodynamics

The two-dimensional unsteady aerodynamic behavior of airfoils described in this section is based on the work of Leishman and Beddoes [8, 9, 10, 11, 12]. The formulation can be separated into two components: the unsteady behavior of the attached flow and the separated flow behavior. These two aspects of the problem will be treated separately in sections 7.1 and 7.2, respectively.

7.1 Unsteady attached flow

The formulation of the unsteady behavior of the attached flow leads to the following set of first order ordinary differential equations

$$\dot{\underline{x}} = \underline{\underline{A}}\,\underline{x} + \underline{\underline{B}}\,\underline{u}, \tag{94a}$$

$$\underline{y} = \underline{\underline{C}}\,\underline{x} + \underline{\underline{D}}\,\underline{u}, \tag{94b}$$

where $\underline{u}$ is the input array, $\underline{y}$ the output array, and $\underline{x}^T = \lfloor x_1, x_2, ..., x_8 \rfloor$ the state array.

The relative flow velocity at quarter-chord is given by eq. (7) and its components along unit vectors $\bar{a}_2$ and $\bar{a}_3$ are U_2 an U_3, respectively, as given by eq. (8). The input array is defined as

$$\underline{u}_{2\times 1} = \begin{Bmatrix} \alpha(t) \\ q(t) \end{Bmatrix}, \tag{95}$$

where $\alpha = \arctan(U_3/U_2)$ is the angle of attack measured in radians from the zero-lift line, as shown in fig. 3, and $q = \dot{\alpha}c/V$ the normalized pitch rate, counted positive for nose-up rotation. The output array is defined as

$$\underline{y}_{2\times 1} = \begin{Bmatrix} C_N^p(t) \\ C_M(t) \end{Bmatrix}, \tag{96}$$

where C_N^P is the normal force coefficient under potential flow conditions, and C_M the quarter-chord pitching moment coefficient.

Once a solution has been obtained for theses two coefficients, the effective angle of attack of the airfoil due to the shed wake (circulatory) terms can be written in terms of the states x_1 and x_2 as

$$\alpha_E(t) = \bar{V}\beta^2(A_1 b_1 x_1 + A_2 b_2 x_2), \tag{97}$$

where b is the semi-chord length and M the Mach number. The Prandtl-Glauert compressibility factor is $\beta = \sqrt{1-M^2}$ and $\bar{V} = V/b$.

The chord force and pressure drag coefficients, as shown in fig. 12, are then found as

$$C_c(t) = \eta\,\bar{C}_{N_\alpha}\alpha_E^2(t), \tag{98a}$$

$$C_D(t) = C_N^p \sin\alpha - C_c\cos\alpha, \tag{98b}$$

respectively. The total section drag is obtained by adding the profile drag forces, as described in section 4.3.

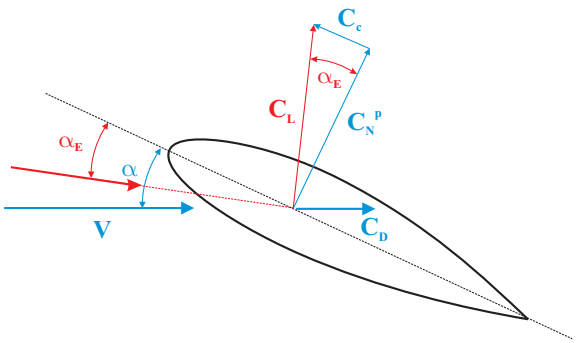

Figure 12: Definition of the chord force and pressure drag coefficients.

The coefficients appearing in the above equations are defined as follows.

1. The governing equations, eqs. (94), involve the four matrices defined here. First, the diagonal matrix $\underline{\underline{A}}$ is defined as

$$\underline{\underline{A}}_{8\times 8} = -\mathrm{diag}\left(\bar{V}\beta^2 b_1, \bar{V}\beta^2 b_2, \frac{1}{T_{N_\alpha}}, \frac{1}{T_{N_q}}, \frac{1}{b_3 T_{M_\alpha}}, \frac{1}{b_4 T_{M_\alpha}}, \bar{V}\beta^2 b_5, \frac{1}{T_{M_q}}\right). \tag{99}$$

Next, the rectangular matrices $\underline{\underline{B}}$ and $\underline{\underline{C}}$ are defined as

$$\underline{\underline{B}}_{8\times 2} = \begin{bmatrix} 1 & 0.5 \\ 1 & 0.5 \\ 1 & 0 \\ 0 & 1 \\ 1 & 0 \\ 1 & 0 \\ 0 & 1 \\ 0 & 1 \end{bmatrix}, \text{ and } \underline{\underline{C}}^T_{2\times 8} = \begin{bmatrix} \bar{C}_{N_\alpha}\bar{V}\beta^2 A_1 b_1 & (0.25 - x_{ac})\bar{C}_{N_\alpha}\bar{V}\beta^2 A_1 b_1 \\ \bar{C}_{N_\alpha}\bar{V}\beta^2 A_2 b_2 & (0.25 - x_{ac})\bar{C}_{N_\alpha}\bar{V}\beta^2 A_2 b_2 \\ -4/(MT_{N_\alpha}) & 0 \\ -1/(MT_{N_q}) & 0 \\ 0 & A_3/(Mb_3 T_{M_\alpha}) \\ 0 & A_4/(Mb_4 T_{M_\alpha}) \\ 0 & -\pi A_5 b_5 \beta\bar{V}/8 \\ 0 & 7/(12MT_{M_q}) \end{bmatrix}, \tag{100}$$

respectively. Finally, the square matrix $\underline{\underline{D}}$ is

$$\underline{\underline{D}}_{2\times 2} = \frac{1}{M}\begin{bmatrix} 4 & 1 \\ -(A_3+A_4) & -7/12 \end{bmatrix}. \tag{101}$$

2. $\bar{C}_{N_\alpha}(M)$ is the slope of the lift curve, $x_{ac}(M)$ the aerodynamic center, and η recovery factor for viscosity effect. Typically $\eta \approx 0.95$, for inviscid flow $\eta = 1$.

3. The coefficients of circulatory indicial response functions are denoted $A_i, i = 1, 2, \ldots, 5$. In the absence of unsteady test data, the values of these coefficients can be taken from refs. [11, 12], as shown in Table 2 which lists different sets of coefficients from various sources. Note that $A_1 + A_2 = 1$.

Data Source	A_1	A_2	A_3	A_4	A_5
Boeing Data	0.636	0.364	1.5	-0.5	1.0
ARA Data	0.625	0.375	1.5	-0.5	1.0
NASA Data	0.482	0.518	1.5	-0.5	1.0
Consolidated Data	0.918	0.082	1.5	-0.5	1.0

Table 2: Indicial response coefficients

The Boeing data was obtained from unsteady test run in a 4×4 ft wind tunnel for free-stream Mach numbers of 0.2, 0.4, and 0.6 and for fairly wide range of reduced frequencies. Two airfoil shapes were included in the study: the symmetric NACA 0012 airfoil and the cambered NACA 23010 airfoil. This data is quite unique since a few measurements were made at the very high reduced frequency of 0.72, albeit at lowest Mach number.

On the other hand, the ARA data was obtained from unsteady test run in an 18×8 in intermittent blowdown wind tunnel for the NACA 0012 airfoil. The data covers a range of Mach numbers from 0.3 to 0.75, but only up to reduced frequencies 0.25. Nevertheless, relatively high reduced frequencies were tested at higher Mach numbers of 0.7 and 0.75.

The NASA data was obtained by Davis and Malcolm [13] from the NASA facility for a supercritical NACA 64A010 airfoil. This data was recorded for Mach numbers of 0.5 and 0.8, and for small angle of attack oscillations at reduced frequencies up to 0.3.

4. The exponents or poles of circulatory indicial response functions are denoted $b_i, i = 1, 2, \ldots, 5$. In the absence of unsteady test data, the values of these coefficients can be taken from refs. [11, 12], as shown in Table 3 which lists different sets of coefficients from same sources mentioned previously.

Data Source	b_1	b_2	b_3	b_4	b_5
Boeing Data	0.339	0.249	0.25	0.1	0.5
ARA Data	0.310	0.312	0.25	0.1	0.5
NASA Data	0.684	0.235	0.25	0.1	0.5
Consolidated Data	0.366	0.102	0.25	0.1	0.5

Table 3: Indicial response coefficients

It is clear from Tables 2 and 3 that the indicial response coefficients and exponents strongly depend on the actual experimental data set used. Thus, in view of the limited data from any source, the results from the various tests were consolidated into one data set which covers Mach numbers from 0.2 up to 0.8, and is mainly for reduced frequencies up to 0.3.

Also, from ref. [14], the following values can be used: $A_1 = 0.3, A_2 = 0.7, b_1 = 0.14$ and $b_2 = 0.53$ and their generalization to different Mach numbers is done through the scaling of the exponents by β^2. This will be used in the implementation of the model.

5. The non-circulatory time constant multiplier are denoted $k_{N_\alpha}, k_{N_q}, k_{M_\alpha}$ and k_{M_q}. In the absence of available unsteady test data, the following empirical data can be used $k_{N_\alpha} \approx 0.75$, $k_{N_q} \approx 0.75$, $k_{M_\alpha} \approx 0.8$ and $k_{M_q} \approx 0.8$.

6. The non-circulatory time constants

$$T_I = \frac{2b}{c_s} \tag{102}$$

$$K_{N_\alpha} = \frac{k_{N_\alpha}}{(1-M) + \pi\beta M^2 \sum_{i=1}^{2} A_i b_i}, \qquad T_{N_\alpha} = K_{N_\alpha} T_I \tag{103}$$

$$K_{N_q} = \frac{k_{N_q}}{0.5(1-M) + 2\pi\beta M^2 \sum_{i=1}^{2} A_i b_i}, \qquad T_{N_q} = K_{N_q} T_I \tag{104}$$

$$K_{M_\alpha} = \frac{k_{M_\alpha}(A_3 b_4 + A_4 b_3)}{b_3 b_4 (1-M)}, \qquad T_{M_\alpha} = K_{M_\alpha} T_I \tag{105}$$

$$K_{M_q} = \frac{7 k_{M_q}}{15(1-M) + 3\pi\beta M^2 A_5 b_5}, \qquad T_{M_q} = K_{M_q} T_I \tag{106}$$

where c_s is the speed of sound and.

7.2 Separated flow behavior

To solve for the separated flow behavior, we need to add the following inputs, where in the absence of available test data, there values can be taken from Table 4. This theory for separated flow and dynamic stall model is presented in refs. [8, 9, 15].

1. $\alpha_1,\ S_1,\ S_2$;

   From the airfoil static $C_N - \alpha$ data, we can compute the corresponding trailing edge separation point f (as fraction of the airfoil chord) using the following relation:

$$f = \left[2\sqrt{\frac{C_N}{\bar{C}_{N_\alpha}(M)\alpha}} - 1 \right]^2 \tag{107}$$

   Then we can curve fit $f - \alpha$ static relation to two expressions, before and after the static stall, as following:

$$f = \begin{cases} 1 - 0.3\,\exp((\alpha - \alpha_1)/S_1) & \alpha \le \alpha_1, \\ 0.04 + 0.66\,\exp((\alpha_1 - \alpha)/S_2) & \alpha > \alpha_1. \end{cases} \tag{108}$$

   where S_1, S_2 and α_1 are three empirical parameters which may be fitted to the test data. α_1 is the break point corresponding to $f \approx 0.7$ (closely correspond to the static stall angle of attack for most airfoil sections). There values in Table 4 are in degrees (and are input to the model also in degrees).

   However, this relation must be modified to account for negative angle of attack, as shown in ref. [7]

$$f = \begin{cases} 1 - 0.3\,\exp((|\alpha| - \alpha_1)/S_1) & |\alpha| \le \alpha_1, \\ 0.04 + 0.66\,\exp((\alpha_1 - |\alpha|)/S_2) & |\alpha| > \alpha_1. \end{cases} \tag{109}$$

2. $k_0,\ k_1,\ k_2,\ m$;

   From the airfoil static test data we can compute C_M/C_N ratio. For the same angles of attack we have f (obtained as mentioned previously), then we can curve fit their relation to:

$$C_M/C_N = k_0 + k_1(1-f) + k_2\,\sin(\pi f^m) \tag{110}$$

   where: $k_0 = (0.25 - x_{ac})$ is aerodynamic center offset from the quarter chord (x_{ac} is one of the inputs to the attached flow module (7.1)), k_1 represents the direct effect on the center of pressure due to the growth of the separated flow region, and k_2 helps describe the shape of the moment break at stall.

   The values of k_0, k_1, k_2 and m can be adjust to give the best moment reconstruction. m will be taken equal to 2.0 in the implementation of the model.

3. $T_p(M)$ and $T_f(M)$ which are Mach number dependent time constants used in the separated flow behavior.

   As in the case of T_p, T_f is albeit weaker mach number dependent. It appears that the values of T_p are largely independent of airfoil shape. While it is more difficult to determine how T_f changes with airfoil shape. Without access to unsteady airfoil data, an unsteady boundary layer code can be practically used to determine how T_f varies with airfoil shape.

M	0.30	0.40	0.50	0.60	0.70	0.75	0.80	Units
α_1	15.25	12.5	10.5	8.5	5.6	3.5	0.7	deg.
$\delta\alpha_1$	2.1	2.0	1.45	1.0	0.8	0.2	0.1	deg.
S_1	3.0	3.25	3.5	4.0	4.5	3.5	0.7	deg.
S_2	2.3	1.6	1.2	0.7	0.5	0.8	0.18	deg.
k_0	0.0025	0.006	0.02	0.038	0.03	0.001	-0.01	non-dim.
k_1	-0.135	-0.135	-0.125	-0.12	-0.09	-0.13	0.02	non-dim.
k_2	0.04	0.05	0.04	0.04	0.15	-0.02	-0.01	non-dim.
T_p	1.7	1.8	2.0	2.5	3.0	3.3	4.3	non-dim.
T_f	3.0	2.5	2.2	2.0	2.0	2.0	2.0	non-dim.

Table 4: Airfoil coefficients for unsteady separated flow modeling, as functions of M, for NACA 0012

Now, to go through the following sections, we need to split down the components of the output vector $\underline{y}$, eq.(96), into their circulatory and noncirculatory parts , and define each as function of the states or their time derivatives

$$\underline{y} = \begin{bmatrix} C_N^p(t) \\ \\ C_M(t) \end{bmatrix} = \begin{bmatrix} C_N^C(t) + C_{N_\alpha}^I(t) + C_{N_q}^I(t) \\ \\ C_{M_\alpha}^C(t) + C_{M_\alpha}^I(t) + C_{M_q}^C(t) + C_{M_q}^I(t) \end{bmatrix}. \tag{111}$$

where

$$C_N^C(t) = \bar{C}_{N_\alpha}\alpha_E(t) \tag{112}$$

$$C_{N_\alpha}^I(t) = \frac{4}{M}\dot{x}_3. \tag{113}$$

$$C_{N_q}^I(t) = \frac{1}{M}\dot{x}_4. \tag{114}$$

$$C_{M_\alpha}^C(t) = k_0 C_{N_\alpha}^C(t). \tag{115}$$

$$C_{M_\alpha}^I(t) = \left(\frac{-1}{M}\right)\left[A_3\dot{x}_5 + A_4\dot{x}_6\right]. \tag{116}$$

$$C_{M_q}^C(t) = \left(\frac{-\pi A_5 b_5 \beta V}{8b}\right) x_7. \tag{117}$$

$$C_{M_q}^I(t) = \left(\frac{-7}{12M}\right)\dot{x}_8. \tag{118}$$

The time derivatives of the states are taken from eq.(94). Note that we can calculate only the circulatory or the noncirculatory part of C_N^p and C_M as previously shown, then use eq.(111) to get the other part.
Define $C_{N_\alpha}^C(t)$ as the circulatory part of the normal force coefficient due to angle of attack only, i.e. it is calculated similarly to eqs.(97, 112) as

$$C_{N_\alpha}^C(t) = \bar{C}_{N_\alpha}\beta^2\left(\frac{V}{b}\right)(A_1 b_1 \widehat{x}_1 + A_2 b_2 \widehat{x}_2). \tag{119}$$

where these two new states are get from

$$\dot{\widehat{x}}_i = A(i,i)\widehat{x}_i + \alpha(t), i = 1, 2. \tag{120}$$

where $A(i,i)$ is the i^{th} diagonal term of matrix A (eq.(99)). Also they can be computed numerically from the corresponding first two states of the attached flow solution, by extracting the effect of the pitch rate $q(t)$ input.

7.2.1 Leading edge separation effect

Under unsteady conditions, normal force coefficient $C_N(t)$ lag $\alpha(t)$, and the leading edge pressure response lag $C_N(t)$; therefore the critical pressure for separation onset (stall) at the appropriate mach number is achieved at a higher angle of attack then the quasi-static case, and there is an overall delay in the onset of dynamic stall.

To implement the critical pressure criterion under unsteady conditions, a 1^{rst} order lag is applied to $C_N^p(t)$ to produce a subsonic value $C_N'(t)$

$$D_{p_n} = D_{p_{n-1}}E_p + (C_{N_n}^C - C_{N_{n-1}}^C)E_p^{0.5}. \tag{121}$$

where

$$E_p = \exp\left(\frac{-\Delta S}{T_p}\right) \tag{122}$$

then

$$C'_{N_n} = C^p_{N_n} - D_{p_n}. \tag{123}$$

where n is the current time sample, $S = Vt/b$ is the non-dimensional distance traveled by airfoil in semi-chords, $\Delta S = S_n - S_{n-1}$, and $C^p_{N_n}$ is the total unsteady normal force coefficient for attached flow. The equation for C'_{N_n} can be written in the form of a state equation as ref. [15]

$$\dot{x}_9 = \left(\frac{-x_9}{T_p}\right) + \left(\frac{C^p_N(t)}{T_p}\right). \tag{124}$$

$$C'_N(t) = x_9. \tag{125}$$

7.2.2 Trailing edge separation effect

There exist a modified trailing edge separation point location due to temporal effects on the airfoil pressure distribution and the boundary layer response. An open loop procedure is developed to represent the time dependent effects on the trailing edge separation point f, eq. (108), and thereby permits the evaluation of nonlinear forces and moments under dynamic conditions via the application of *Kirchhoff* theory. The procedure is performed by

1. First, define an effective angle of attack, $\alpha_f(t)$, which gives the same unsteady leading edge pressure as for the equivalent quasi-steady case

$$\alpha_f(t) = \frac{C'_N(t)}{\bar{C}_{N_\alpha}(M)}. \tag{126}$$

2. Using this effective angle of attack, determine a value for the trailing edge separation point, f', from the static $\alpha - f$ relationship (108). However, the static hysteresis around stall when the angle of attack is decreasing, is modeled using an empirically derived dynamic offset, $\Delta\alpha_{1_n}$, formulated as ref. [8]

$$\Delta\alpha_{1_n} = \begin{cases} \left((1 - f''_{n-1})^{0.25}\delta\alpha_1\right) & S_\alpha < 0 \\ 0 & S_\alpha >= 0 \end{cases} \tag{127}$$

where
$\delta\alpha_1$ is function of the airfoil and Mach number, as given in degrees in Table 4.
$S_\alpha = (\alpha_n - \alpha_{n-1})$ is used to detect the angle of attack is increasing or decreasing with time (pitch up or down). Note that the unsteady T.E. separation point f'' used here is from the previous time step (eq. (132)). Then α_1 used to calculate f', is calculated as

$$\alpha_{1_n} = \alpha_1 - \Delta\alpha_{1_n}. \tag{128}$$

then

$$f' = \begin{cases} 1 - 0.3\,\exp\left[(|\alpha_f| - \alpha_{1_n})/S_1\right] & |\alpha_f| \le \alpha_{1_n} \\ 0.04 + 0.66\,\exp\left[(\alpha_{1_n} - |\alpha_f|)/\,S_2\right] & |\alpha_f| > \alpha_{1_n} \end{cases} \tag{129}$$

3. Additional effects of the unsteady boundary layer response may be represented by applying a first-order lag to f' to produce final value for the unsteady trailing edge separation point f''. The deficiency function is given by

$$D_{f_n} = D_{f_{n-1}}E_f + (f'_n - f'_{n-1})E_f^{0.5}. \tag{130}$$

where

$$E_f = \exp\left(\frac{-\sigma_1\Delta S}{T_f}\right) \tag{131}$$

where $\sigma_i,\ \ i = 1, 2, 3$ are three time constants parameters, and their values will be specified at each time step, in order to solve the interaction between the different flow features.
Then, we can calculate the dynamic T.E. separation point as

$$f''_n = f'_n - D_{f_n}. \tag{132}$$

Alternatively, this additional lag in the T.E. separation point can be represented in state space equation as ref. [15]

$$\dot{x}_{10} = \left(\frac{-x_{10}}{T_f}\right) + \left(\frac{f'(t)}{T_f}\right). \tag{133}$$

$$f''(t) = x_{10}. \tag{134}$$

4. Finally, the nonlinear normal force coefficient C_N^f, incorporating the effect of the unsteady trailing edge separation point f'', can be given by

$$C_{N_n}^f = C_{N_n}^{fC} + C_{N_n}^I. \tag{135}$$

where $C_{N_n}^{fC}$ being the circulatory part of the normal force coefficient, including the separated flow effect, computed as

$$C_{N_n}^{fC} = K_{N_n} C_{N_n}^C. \tag{136}$$

$$K_{N_n} = \frac{(1+\sqrt{f_n''})^2}{4}. \tag{137}$$

and the noncirculatory normal force coefficient computed from eqs. (113) and (114) as

$$C_{N_n}^I = C_{N_{\alpha_n}}^I + C_{N_{q_n}}^I. \tag{138}$$

Similarly, the pitching moment coefficient is given by

$$C_{M_n}^f = \left[k_0 + k_1(1-f_n'') + k_2 \sin(\pi f_n^{"m})\right] C_{N_{\alpha_n}}^{fC} + C_{M_{q_n}}^C + C_{M_n}^I + C_{M_0}. \tag{139}$$

where C_{M_0} the zero lift pitching moment, and $C_{N_{\alpha_n}}^{fC}$ being the circulatory part of the normal force coefficient due to angle of attack only, including the separated flow effect, computed from eq. (120), similarly to eq. (136), as

$$C_{N_{\alpha_n}}^{fC} = K_{N_n} C_{N_{\alpha_n}}^C. \tag{140}$$

and the noncirculatory moment coefficient computed from eqs.(116, 118) as

$$C_{M_n}^I = C_{M_{\alpha_n}}^I + C_{M_{qn}}^I. \tag{141}$$

Finally, the chord force and pressure drag coefficients, for the separated flow, are given respectively as

$$C_{c_n}^f = \eta\, \bar{C}_{N_\alpha}(M) \alpha_{E_n}^2 \sqrt{f_n''}. \tag{142}$$

$$C_{D_n}^f = C_{N_n}^f \sin\alpha - C_{c_n}^f \cos\alpha. \tag{143}$$

If the vortex effect is to be added, then we will go to next section. However, if wanted only the effect of the T.E. separation point, then the total section drag is obtained by adding the profile drag forces, as described in section 4.3.

7.2.3 Dynamic stall effect:

This model take its input from the previous two sections for unsteady aerodynamic attached and separated flow. We need to add the following inputs, where in the absence of available unsteady test data, there values can be taken from Table 5.

1. C_{N_1};
   From an analysis of airfoil static test data, the critical normal force coefficient C_{N_1}, may be obtained which corresponds to the critical pressure for separation onset at the appropriate Mach number. In practice, it can be obtained from the value of $C_{N(static)}$ that corresponds to either the break in pitching moment or the chord force at stall ref. [9].

2. $T_v(M)$ and $T_{vl}(M)$;
   The vortex decay constant, $T_v(M)$, and the center of pressure travel time constant, $T_{vl}(M)$, appear in Table 5 relatively independent of Mach number over most of the mach number range. The dynamic stall experiments show that while there is a significant effect of airfoil shape under light stall conditions, all airfoils behave similarly under strong dynamic stall conditions. Thus, it can be concluded that the parameters T_v and T_{vl} should be relatively insensitive to airfoil shape.

M	0.30	0.40	0.50	0.60	0.70	0.75	0.80	Units
C_{N_1}	1.45	1.2	1.05	0.92	0.68	0.5	0.18	non-dim.
T_v	6.0	6.0	6.0	6.0	6.0	6.0	4.0	non-dim.
T_{vl}	7.0	9.0	9.0	9.0	9.0	9.0	9.0	non-dim.
Df	8.0	7.75	6.2	6.0	5.9	5.5	4.0	non-dim.

Table 5: Airfoil coefficients for dynamic stall modeling, as functions of M, for NACA 0012

3. Df;
   This constant models empirically the increased rate at which the chord force is lost (and hence the onset of drag divergence) after the onset of the gross separation of flow in dynamic stall.

The general case of dynamic stall involves the formation of a vortex near the airfoil leading edge, which at certain point, separates and convects downstream. The onset of leading edge separation for subcritical flow, or shock induced separation for higher Mach number flow, under dynamic conditions will be initiated when $C'_N(t)$ eq. (123) exceeds the critical $C_{N_1}(M)$ boundary.

At this point there is a catastrophic loss of the leading edge suction, and the accumulated vortex lift is assumed to start to convect over the airfoil chord ref. [15]. Then τ_v, a non-dimensional vortex time parameter (in semi-chords), is used to track the position of the convected vortex such that $\tau_v = 0$ at the onset of separation conditions, and $\tau_v = T_{vl}$ when the vortex reaches the trailing edge. It is computed from eq. (164). Experimental tests ref. [9] show that the rate of vortex convection is less then half the free-stream velocity, with weak dependence on the Mach number. Vortex speed can be calculated as ref. [7] $V_{vortex} = 2V/T_{vl}$.

For discretely sampled system, the vortex lift force coefficient C_N^v is represented by assuming that, for a given sample period, the increment in vortex lift C_v is determined by

$$C_{v_n} = D_s C_{N_n}^C (1 - K_{N_n}). \tag{144}$$

where K_{N_n} is from eq. (137), and $C_{N_n}^C$ from eq. (112). Then the total accumulated vortex lift can be calculated from

$$C_{N_n}^v = C_{N_{n-1}}^v E_v + D_s (C_{v_n} - C_{v_{n-1}}) E_v^{0.5} \tag{145}$$

where

$$E_v = \exp\left(\frac{-\sigma_2 \Delta S}{T_v}.\right) \tag{146}$$

D_s is a switch that takes at the beginning its value from the previous time step, and after that its value is zero, unless any of the following conditions is met, where it equals unity, refs. [15, 7].

1. $0 < \tau_v \leq T_{vl}$; or
2. $|C'_N| < C_{N_1}$ and $\Delta f'' < 0$; or
3. $S_\alpha > 0$ and $\Delta f'' > 0$.

where
τ_v is a the non-dimensional vortex time parameter,
$\Delta f'' = \left(f''_n - f''_{n-1}\right)$ is computed at the end of the time step to be used for the next one, in order to detect the flow is separating, $\Delta f'' < 0$, or reattaching, i.e. $\Delta f'' > 0$.
Alternatively, the accumulated vortex lift can be calculated from the following state space form ref. [15]

$$\dot{x}_{11} = \left(\frac{-x_{11}}{T_v}\right) + D_s \left(\frac{\dot{C}_v}{T_v}\right). \tag{147}$$

$$C_N^v(t) = x_{11}. \tag{148}$$

Based on analysis of experimental data involving dynamic stall over wide range of mach number, a representation of the center of pressure behavior (aft quarter-chord) was formulated empirically, if $(0 < \tau_v <= 2T_{vl})$, as

$$CP_v = 0.25\left(1 - \cos(\frac{\pi \tau_v}{T_{vl}})\right). \tag{149}$$

otherwise its default value is 0.
Finally, the increment in pitching moment about the quarter-chord due to the aft-moving center of pressure is given by

$$C_M^v = -CP_v C_N^v. \tag{150}$$

From the above, the total loading can be get by superposition. The total normal force and pitching moment coefficients under dynamic stall conditions are given by

$$C_N(t) = C_N^f(t) + C_N^v(t). \tag{151}$$

$$C_M(t) = C_M^f(t) + C_M^v(t). \tag{152}$$

After onset of gross separation, *Kirchhoff* modification for the chord force eq. (142) becomes invalid, and another procedure, that ensure the continuity of its behavior, is used

$$C_{c_n} = \eta \bar{C}_{N_\alpha}(M)\alpha_{E_n}^2 \sqrt{f_n''}\,\Phi \tag{153}$$

where Φ, taking a maximum value of unity, is defined by

$$\Phi = \begin{cases} 1 & |C_N'| \le C_{N_1} \\ f_n''^{min(Df(|C_N'|-C_{N_1}),1)} & |C_N'| > C_{N_1} \end{cases} \tag{154}$$

where the constant Df values for different Mach numbers can be taken from Table 5.

The pressure drag coefficient, as shown in fig. 12, is then found similarly to eq.(143)

$$C_D(t) = C_N(t)\sin\alpha - C_c(t)\cos\alpha, \tag{155}$$

As mentioned before, the total section drag is obtained by adding the profile drag forces, as described in section 4.3.

7.2.4 Flow reattachment:

Flow is allowed to reattach from deep stall after a reasonable time delay $\tau_v > 2T_{vl}$, during the presence of the vortex. However, this is superseded whenever $|C_N'(t)| < C_{N_1}$. The modification of the model during reattachment will be done through modification of the time constants parameters: σ_1, σ_2 and σ_3, as will be shown in the next section. In addition, the pitching moment coefficient is calculated using a different T.E. separation point f_{qs}, which is a quasi steady value. Thus, for $C_M(t)$ calculation, we have (refs. [8, 16])

$$f_M^r = \begin{cases} f' & S_\alpha \ge 0 \\ f_{qs} & S_\alpha < 0 \end{cases}. \tag{156}$$

where

$$f_{qs} = \begin{cases} 1 - 0.3\,\exp\left[(|\alpha| - \alpha_{1_n})/S_1\right] & |\alpha| \le \alpha_{1_n} \\ 0.04 + 0.66\,\exp\left[(\alpha_{1_n} - |\alpha|)/\,S_2\right] & |\alpha| > \alpha_{1_n} \end{cases}. \tag{157}$$

then

$$D_{f_n}^r = D_{f_{n-1}}^r E_m + (f_{M_n}^r - f_{M_{n-1}}^r)E_m^{0.5} \tag{158}$$

where

$$E_m = \exp\left(\frac{-\sigma_3 \Delta S}{T_f}\right). \tag{159}$$

then

$$f_n''^r = f_{M_n}^r - D_{f_n}^r. \tag{160}$$

and the pitching moment coefficient, similarly to eq.(139) is given by

$$C_{M_n}^f = [k_0 + k_1(1 - f_n''^r) + k_2 \sin(\pi(f_n''^r)^m)]\, K_{Nr_n} C_{N_{\alpha n}}^C + C_{M_{qn}}^C + C_{M_n}^I + C_{M_0}. \tag{161}$$

where

$$K_{Nr_n} = \frac{(1 + \sqrt{f_n''^r})^2}{4}. \tag{162}$$

7.2.5 Time constants modification:

As mentioned before, in order to solve the interaction between the different parts of the theory, the Time constants T_f and T_v will be modified at each time step, through the values of their parameters σ_1, σ_2 and σ_3 (with two different parameters for T_f for both the force and the moment coefficients, for allowing different behavior during reattachment).

Their default values are: $\sigma_1 = 1, \sigma_2 = 1$ and $\sigma_3 = 5$. Note that at the beginning of each time step, their values from previous time step will be used, then updated at its end.

Their values will be determined based on the flow is separating or reattaching, i.e. the sign of $\Delta f''$, the angle of attack is increasing or decreasing, i.e. the sign of S_α, and on the phase of the flow itself, as shown next refs. [8, 16, 7].

if $(|C_N'| < C_{N_1})$
  FlagState = 0
  if $(\Delta f'' \le 0)$
    $\sigma_1 = \sigma_3 = 1.$
  else

$\sigma_1 = 0.5,\ \sigma_3 = 5.$
end
elseif $(|C'_N| \geq C_{N_1})$
FlagState $= 1$
if $(\Delta f'' \leq 0)$
$\sigma_1 = \sigma_3 = 1.75.$
else
$\sigma_1 = 1.0,\ \sigma_3 = 5.$
if $(0 < \tau_v \leq T_{vl})$
$\sigma_1 = 0.25.$
if $(S_\alpha > 0)$
$\sigma_1 = 0.75.$
end
end
end
end

Then the following test is performed

if $(|C'_N| > C_{N_1}\ \&\ \Delta f'' \leq 0)$
if ($S_\alpha < 0$ or $f'' \leq 0.7$ or $f''^r \leq 0.7$)
$\sigma_1 = \sigma_3 = 2.0.$
end
end

where FlagState is used to determine the initiation of dynamic stall phase ($|C'_N| \geq C_{N_1}$), in order to compute the non-dimensional vortex travel time τ_v, which has default value equals to 0, then at the first instant of the onset of the dynamic stall, its initial value is computed as (ref.([7]))

$$\tau_v = \Delta t \left(\frac{V}{b}\right) \left(\frac{|C'_{N_n}| - C_{N_1}}{|C'_{N_n}| - |C'_{N_{n-1}}|}\right). \tag{163}$$

where V is the relative flow velocity in the plane of the airfoil as given by eq. (11). After that, its accumulation during vortex travel, as long as $FlagState = 1$, is computed simply from

$$\tau_{v_n} = \tau_{v_{n-1}} + \Delta t \frac{V}{b}. \tag{164}$$

Now, for the dynamic stall model, the determination of the value of σ_2 will be as follows

if $(S_\alpha < 0)$
$\sigma_2 = 4.0.$
elseif $(T_{vl} < \tau_v \leq 2T_{vl})$
$\sigma_2 = 3.0.$
elseif $(\Delta f'' > 0)$
$\sigma_2 = 4.0$.
elseif $(0 < \tau_v \leq T_{vl}\ \&\ S_\alpha < 0)$
$\sigma_2 = 2.0.$
elseif $(S_\alpha < 0\ \&\ \sigma_2 = 1.0)$
$\sigma_2 = 4.0.$
elseif $(S_\alpha < 0\ \&\ \Delta f'' > 0)$
$\sigma_2 = 1.0.$
end

8 Unsteady Aerodynamic solution options

For the unsteady attached flow aerodynamics theories we have: Peters unsteady aerodynamics and Leishman-Beddoes. For the Dynamic stall we have Leishman-Beddoes theory and *ONERA EDLIN* model. For their combination we have the following options:

1. Attached Flow solution

(a) Peters unsteady aerodynamics theory developed in section 3.

(b) Leishman-Beddoes unsteady aerodynamics theory developed in section 7.

2. Separated Flow solution

(a) Peters unstated aerodynamics theory with *ONERA EDLIN* dynamic stall model (6). The results are the addition of the corresponding eqs. (53) and eqs. (87).

(b) Leishman-Beddoes separated flow (7.2). Its results are from eq. (135) to eq. (143), and eq. (161). After that we will have the option to add the vortex loads or not. In case of including the vortex effect, then the results are from eq. (151) to eq. (155), and eq. (161). Summary of the I/O stream for each of Leishman-Beddoes modules, is shown in fig. 13.

Note that for the separated flow solution, if it is selected not to add the dynamic stall vortex effect, then the input data for this module will be turned off, except C_{N_1} (used for the modification of Time constant parameters σ_1 and σ_3). Similarly, if selected only the attached flow solution, then the required data for both the separated flow and the dynamic stall vortex effect (7.2.3), will be turned off.

References

[1] K.J. Bathe. *Finite Element Procedures*. Prentice Hall, Inc., Englewood Cliffs, New Jersey, 1996.

[2] D.A. Peters and M.J. Johnson. Finite state airloads for deformable airfoils on fixed and rotating wings. In *Proceedings of the Symposium on Aeroelasticity and Fluid/Structure Interaction*. American Society of Mechanical Engineers Winter Annual Meeting, Nov. 1994.

[3] D.A. Peters, M.A. Hsieh, and A. Torrero. A state-space airloads theory for flexible airfoils. *Journal of the American Helicopter Society*, 52(4):329–342, October 2007.

[4] L.A. Ahaus and D.A. Peters. Unified airloads model for morphing aifoils in dynamic stall. In *Proceedings of the AHS Specialist's Conference on Aeromechanics*, San Francisco, 2010.

[5] R.L. Bisplinghoff, H. Ashley, and R.L. Halfman. *Aeroelasticity*. Addison-Wesley Publishing Company, Reading, Massachusetts, second edition, 1955.

[6] D. Petot. Differential equation modeling of dynamic stall. *La Recherche Aérospatiale*, 5:60–72, 1989.

[7] W. Johnson. CAMRAD II components theory, volume ii. Technical Report Release 3.2, Johnson Aeronautics, Palo Alto, California, June 1999.

[8] J.G. Leishman and T.S. Beddoes. A generalized model for airfoil unsteady behavior and dynamic stall using the indicial method. In *American Helicopter Society 42nd Annual Forum Proceedings*, Washington, DC, June 1986.

[9] J.G. Leishman and T.S. Beddoes. A semi-empirical model for dynamic stall. *Journal of the American Helicopter Society*, 34(3):3–17, July 1989.

[10] J.G. Leishman. *Principles of Helicopter Aerodynamics*. Cambridge University Press, Cambridge, second edition, 2006.

[11] J.G. Leishman. Indicial lift approximations for two-dimensional subsonic flow as obtained from oscillatory measurements. *Journal of Aircraft*, 30(3):340–351, May-June 1993.

[12] J.G. Leishman and K.Q. Nguyen. State-space representation of unsteady airfoil behavior. *AIAA Journal*, 28(5):836–844, May 1990.

[13] S.S. Davis and G.N. Malcolm. Experimental unsteady aerodynamics of conventional and supercritical airfoils. Technical Report TM 81221, NASA, 1980.

[14] T.S. Beddoes. Practical computation of unsteady lift. *Vertica*, 8(1):55–71, 1984.

[15] J.G. Leishman and G.L. Crouse. State-space model for unsteady airfoil behavior and dynamic stall. In *Proceedings of the 30th AIAA/ASME/ASCE/AHS/ASC Structures, Structural Dynamics and Materials Conference, Mobile, Alabama, April 3-5, 1989*, pages 1319–1330, 1989.

[16] Anon. RCAS theory manual, version 2.0. Technical Report USAAMCOM/AFDD TR 02-A-005, U.S. Army Aviation and Missile Command, Moffett Field, California, June 2003.

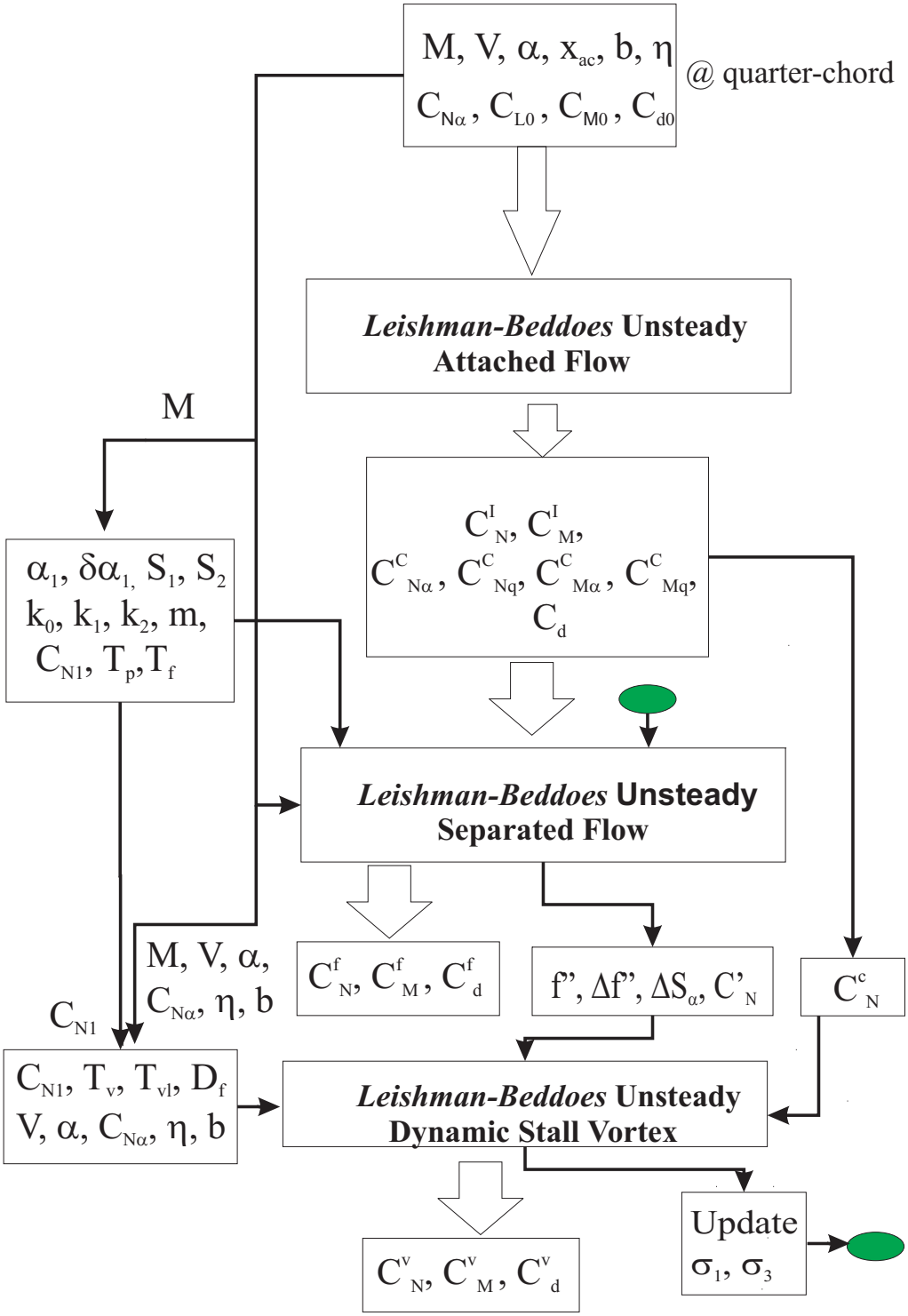

Figure 13: I/O for the complete Leishman-Beddoes Dynamic Stall Model.